NASA

B747/JT9D FLIGHT LOADS AND THEIR EFFECT ON ENGINE RUNNING CLEARANCES AND PERFORMANCE DETERIORATION

NACELLE AERODYNAMIC AND INERTIAL LOADS (NAIL)/ JT9D JET ENGINE DIAGNOSTICS PROGRAMS

W. J. Olsson and R. L. Martin

UNITED TECHNOLOGIES CORPORATION
Pratt & Whitney Aircraft Group
Commercial Products Division

and

Boeing Commercial Airplane Company
A DIVISION OF THE BOEING COMPANY
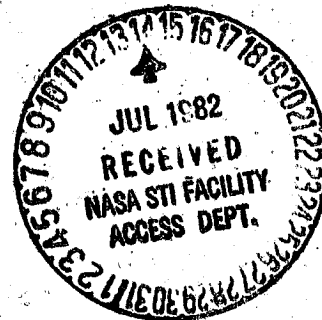
Prepared for

NATIONAL AERONAUTICS AND SPACE ADMINISTRATION

Lewis Research Center
Cleveland, Ohio 44135

1. Report No. NASA CR-165573	2. Government Accession No.	3. Recipient's Catalog No.
4. Title and Subtitle B747/JT9D Flight Loads and their Effect on Engine Running Clearances and Performance Deterioration; BCAC NAIL/P&WA JT9D Engine Diagnostics Programs		5. Report Date February 19, 1982
		6. Performing Organization Code
7. Author(s) W. J. Olsson and R. L. Martin		8. Performing Organization Report No. PWA-5512-88
		10. Work Unit No.
9. Performing Organization Name and Address UNITED TECHNOLOGIES CORPORATION Pratt & Whitney Aircraft Group, Commercial Products Div. & THE BOEING COMPANY, Boeing Commercial Airplane Company		11. Contract or Grant No. NAS3-20632; NAS1-15325
		13. Type of Report and Period Covered Contractor Report
12. Sponsoring Agency Name and Address NATIONAL AERONAUTICS AND SPACE ADMINISTRATION NASA Lewis Research Center NASA Langley Research Center Cleveland, Ohio 44135 Hampton, Virginia 23665		14. Sponsoring Agency Code

15. Supplementary Notes

Project Manager, C. M. Mehalic   Project Manager, D. B. Middleton
NASA Lewis Research Center   NASA Langley Research Center

16. Abstract

The joint Pratt & Whitney Aircraft/Boeing Commercial Airplane Company Flight
Loads Test was the final phase of the NASA sponsored JT9D Jet Engine Diagnostics
Program. Prior test and analysis effort had identified a short-term engine
performance deterioration mode which appeared to occur during predelivery
production airplane acceptance testing and in initial revenue service flights.

This test program duplicated the airplane acceptance testing and representative
flight loads which might be incurred in revenue service. Boeing conducted the
test in a 747 airplane which was instrumented to measure flight conditions,
flight loads on the airplane and test engines, and engine performance. Pratt &
Whitney Aircraft provided the instrumented test engines and monitored the
effects of engine power settings and flight conditions on engine running
clearances, blade-to-seal rubs, and resultant performance deterioration.

The test results confirmed the significance of acceptance testing on performance
deterioration and identified some approaches to improved performance retention.

17. Key Words (Suggested by Author(s)) Nacelle Aerodynamic and Inertial Loads (NAIL) Engine/Module Performance Deterioration Thrust Specific Fuel Consumption (TSFC) JT9D-7A Engine Flight Load Effects	18. Distribution Statement		
19. Security Classif. (of this report) UNCLASSIFIED	20. Security Classif. (of this page) UNCLASSIFIED	21. No. of Pages 78	22. Price*

PREFACE

The requirements of NASA Policy Directive
NPD 2220.4 (September 14, 1970) regarding
the use of SI Units have been waived in
accordance with the provisions of paragraph
5d of that Directive by the Director of
Lewis Research Center.

TABLE OF CONTENTS

PRECEDING PAGE BLANK NOT FILMED

LIST OF ILLUSTRATIONS

LIST OF ILLUSTRATIONS (Continued)

LIST OF TABLES

SECTION 1.0

SUMMARY

This report presents the results of the joint Boeing Commercial Airplane Company (BCAC) and Pratt & Whitney Aircraft (P&WA) test analysis activity which measured flight loads on the 747 propulsion system and resulting JT9D blade to outer airseal running clearances during representative acceptance flight and revenue flight sequences. The resulting rub induced clearance changes and engine performance changes were then analyzed to validate and refine the JT9D-7A short term performance deterioration model.

The nacelle aerodynamic and engine inertial loads were measured during a series of flight tests on the Boeing RA001 test aircraft (747) on two engines by Boeing under NASA-Langley Contract NAS1-15325, and the results are reported in Reference 1. Simultaneously, the running clearance and performance changes were measured on the same engines by Pratt & Whitney Aircraft under NASA-Lewis Contract NAS3-20632, and the results are reported in Reference 2. The correlation of the measured loads and clearance changes were undertaken cooperatively between Boeing and Pratt & Whitney Aircraft to permit an improved understanding of the impact of airplane acceptance testing and typical aircraft maneuvers and operational variables during revenue service on JT9D engine performance deterioration. Additionally, previously developed models used in the prediction of performance deterioration were refined to establish the influence of these engine power and flight load induced running clearance closures on JT9D-7 engine performance deterioration.

The air load data developed in the program will be applicable in nondimensional form to under-wing, high bypass ratio turbofan engine installations involving other airplane and engine combinations. However, it should be noted that the test was conducted using JT9D-7A engines with -200 nacelles; therefore, the measured clearance change results are not necessarily representative of more advanced engine installations.

The results of the tests and subsequent BCAC and P&WA analyses indicated the following with respect to flight loads and the effects on the engine:

o Of the three types of flight loads, namely aerodynamic, inertial and gyroscopic, only the first were significant and had any effect on engine performance. Aerodynamic loads on the fan inlet provided a shear force and bending moment on the fan case which was carried through the engine, deflecting cases throughout the engine. This load on the inlet is caused by the bending of the air stream entering the inlet. Thus the magnitude of the

o aerodynamic load is a function of fan air flow, inlet air angle of attack, and airplane speed. The maximum aerodynamic loads, which were greater than previously predicted by Boeing for earlier analytical studies on the effects of flight loads on performance deterioration, Reference 3, occurred at take-off rotation when the angle of attack was maximum and both fan flow and aircraft speed were high. The loads which were up and slightly outward were essentially equal on both inboard and outboard engines at all flight conditons.

o Running clearances were monitored in the inboard and outboard fan and the first stage of the high-pressure turbine on the inboard engine. Maximum clearance closures in the fans and, it is believed, in the uninstrumented low-pressure compressor stages occurred simultaneously with the maximum aerodynamic load. The maximum fan closures with resulting rubs occurred shortly after take-off rotation. Variations in take-off procedure which permitted reduced fan flow and angle of attack resulted in reduced closure, hence reduced rub strip wear. No fan rubs were observed in the remainder of the typical flight cycle. Neither did possible inertial load conditions such as a hard landing cause rubs.

o Aerodynamic loads also contributed to clearance closures in the high-pressure turbine but to a lesser degree. The prime causes of turbine closure were centrifugal effects and differential thermal expansion between rotor and case. For this reason, the minimum clearance condition in the high-pressure turbine occurred in climb when the thermal expansion, thrust bending, and aerodynamic load effects combined to close the engine clearance at the bottom. Turbine running clearances were not as tight for the remainder of the typical revenue flight cycle. However, high G turns and acceptance test maneuvers, which combined high aerodynamic loads and high power operation, did cause tight turbine clearances.

Based on the results of this Flight Loads Test program, the following recommendations are m. Je relative to current-engine operation and future engine development:

Operation

o Use a 20-degree flap setting at take-off, whenever conditions permit, to reduce the maximum aerodynamic load with a reduction in cold section rubs.

o Use a derated power take-off, when conditions permit, to reduce hot section thermal distortion.

o Minimize high power operation immediately prior to start of take-off to prevent the combination of an increased thermal expansion-induced closure and the maximum load-induced closures at take-off, reducing the possibility of turbine rub.

2

o Minimize the possibility of turbine rubs due to snap accelerations with a hot rotor and cooler case.

o Minimize power level increase during stall warning sequences in production acceptance testing.

Development

o Structurally integrate the engine and nacelle design to reduce both the aerodynamic-load induced and thrust-bending induced closures in both the fan/low-pressure compressor and the high-pressure turbine.

o Investigate possible changes in production engine calibration testing of new and overhauled engines to reduce the time spent at high power and thus reduce high-pressure turbine clearance closure and resulting rubs.

o Develop abradable turbine seals such that rubs caused by the inevitable asymmetric closures will open clearances locally, where required, rather than wear blades and open clearances over the full circumference of the turbine.

o Employ laser clearance monitoring probes to measure compressor and turbine running clearances during engine development testing to better understand symmetric and asymmetric clearance closures and thereby achieve an engine that retains tight running clearances.

3

SECTION 2.0

INTRODUCTION

2.1 BACKGROUND

The rapid rise in the cost of oil since the Organization of Petroleum Exporting Countries (OPEC) oil embargo in 1973 has resulted in a national effort to increase the availability of domestic oil, develop alternate sources of energy, and develop near-term and long-term means to reduce fuel consumption. To counteract the adverse impact of the world-wide fuel crisis on the aviation industry, NASA has initiated the Aircraft Energy Efficiency (ACEE) program. Included in this program are major propulsion projects which are addressing both near-term and long-term goals. The long-term activities are directed toward developing propulsion technology to reduce fuel consumption by at least 12 percent in the late 1980's and an additional 15 percent in the early 1990's. The near-term activities are a part of the Engine Component Improvement (ECI) Project which is directed toward improving the fuel consumption of selected current high bypass ratio turbofan engines and their derivatives by 5 percent over the life of these engines. The Engine Component Improvement project is divided into two subprojects, (1) Performance Improvement and (2) Engine Diagnostics. Performance Improvement is directed toward developing fuel saving component technology for existing engines and their derivatives to be introduced during the 1980 to 1982 time period. Engine Diagnostics is directed toward identifying and quantifying engine performance losses that occur during the engine's service life and developing criteria for minimizing these losses.

The first phase of the Engine Diagnostics project was the gathering, documentation, and analysis of historical data. The resulting information was used to establish performance deterioration trends at the overall engine and module level, establish probable causes contributing to performance deterioration, and identify areas and/or components where corrective action could be taken. That effort was completed in 1978, and the results are reported in Reference 4.

The second phase of the Engine Diagnostics project was directed toward expanding the understanding of engine deterioration by acquiring new in-service engine performance data from a selected sample of JT9D engines. This investigation was conducted during the period from February 1977 to February 1979. The main source of data was the Pan American World Airways JT9D-7A(SP) engines which are installed in their fleet of Boeing 747 Special Performance aircraft. These aircraft were introduced in service beginning in March 1976. Data were obtained from on-the-wing ground tests using expanded engine instrumentation, prerepair and postrepair test stand data, and in-flight cockpit monitored data. That effort was completed in 1979, and the results are reported in Reference 5.

4

The third phase of the Engine Diagnostics project was directed toward understanding the causes of short-term performance deterioration. During the first few flights of an aircraft, the performance of the engine deteriorates relative to its production performance level measured on the test stand. The effort to understand the causes of this phenomenon has been divided into several subphases or activities. The first activity was to test and analytically tear down a low time service engine. This activity was completed in June of 1978, and the results are reported in Reference 6. In summary, the results pointed to clearance changes as the major cause of the performance loss which were probably the result of loads imposed on the engine during flight. The second activity was, therefore, directed toward analytically investigating the impact of flight loads using an existing JT9D/747 Propulsion System NASTRAN Structural Model developed jointly by Pratt & Whitney Aircraft and Boeing prior to initiation of the Engine Diagnostics program. This activity resulted in two reports, References 3 and 7. In summary, these analytical studies confirmed that flight load-induced rubs were a primary cause of short-term performance deterioration and indicated that nacelle inlet aerodynamic pressures during flight maneuvers were a principal cause of these rubs. The last activity during the third phase was a Simulated Aerodynamic Loads Test. For this test, an inlet modified with a mechanical loading device was installed on a JT9D engine that was instrumented to monitor running clearances in the engine. Simulated aerodynamic loads were then applied mechanically through the inlet to the operating engine to simulate various flight maneuvers. Running clearances and engine performance were simultaneously monitored and recorded. The analytical results, as reported in Reference 8, established the effects of the simulated aerodynamic loads on each module of the engine.

2.2 OBJECTIVES

The results available from the first three phases of the Engine Diagnostics Program established the general causes of short-term and long-term engine performance deterioration and the magnitude of each cause. It remained for the Flight Loads Test program to establish the specific flight conditions and maneuvers which cause the engine case and rotor bending loads which, in turn, cause rubs and resulting performance loss. Thus, the specific objectives of this final program phase were:

o To measure aerodynamic and inertia loads during flight;

o To explore the effects of airplane gross weight, sink rate, pitch angle, and various typical maneuvers on nacelle loads;

o To simultaneously measure engine clearance closures and performance changes resulting from these airplane maneuvers;

o To make a final refinement of engine performance deterioration prediction models based on the analytical results; and

5

o To make recommendations to improve propulsion system performance
   retention.

2.3 APPROACH

The selected test approach and degree of instrumentation were the
result of a joint feasibility study (Reference 9) which considered
program goals, prior test results, cost, benefits, availability of test
engines and airplane, and schedule. The result of the feasibility
study was the joint flight test conducted by Boeing Commercial Airplane
Company (BCAC) and Pratt & Whitney Aircraft (P&WA). The Boeing
Commercial Airplane Company effort, Nacelle Aerodynamic and Inertial
Loads (NAIL) project, was funded by NASA-Langley under contract
NAS1-15325. The Pratt & Whitney Aircraft effort was funded by
NASA-Lewis under the JT9D Engine Diagnostics program under contract
NAS3-20632. The selected approach was to use the Boeing test 747
airplane, RA001, shown in Figure 2-1, with the two right hand engines
and nacelles instrumented to simultaneously measure flight conditions,
aerodynamic and inertia loads, engine running clearances, and engine
performance.

Figure 2-1 Flight Test Vehicle - The Boeing test 747, RA001, was
            selected for the flight tests on the basis of cost and
            availability.   (J24018-5)

The spare JT9D-7 engine, serial number P-662204, from RA001 was returned to Pratt & Whitney Aircraft where it was partially disassembled and then reassembled with an analytically built and instrumented fan case and high-pressure turbine. Four laser proximity probes were installed around the fan case to measure fan running clearances. The high-pressure turbine case was modified to permit the installation of laser proximity probes for the measurement of first-stage turbine running clearances. Also installed on the high-pressure turbine case were thermocouples to measure transient and steady state temperatures around the case throughout the flight tests. Finally, the engine was equipped with expanded performance instrumentation to measure engine and engine-module performance before, during, and after the flight tests. These engine instrumentation systems are described in the Pratt & Whitney Aircraft Flight Loads Test program final report (Reference 2).

The analytically built engine was calibrated in a test stand, then shipped to Boeing where it was installed in the number 3 position on the test airplane, as shown in Figure 2-2. The laser clearance monitoring and recording system was connected to a Pratt & Whitney Aircraft read-out and recording system in the test airplane cabin. The temperature and performance instrumentation was connected to the Boeing Airborne Data Analysis and Monitoring System (ADAMS).
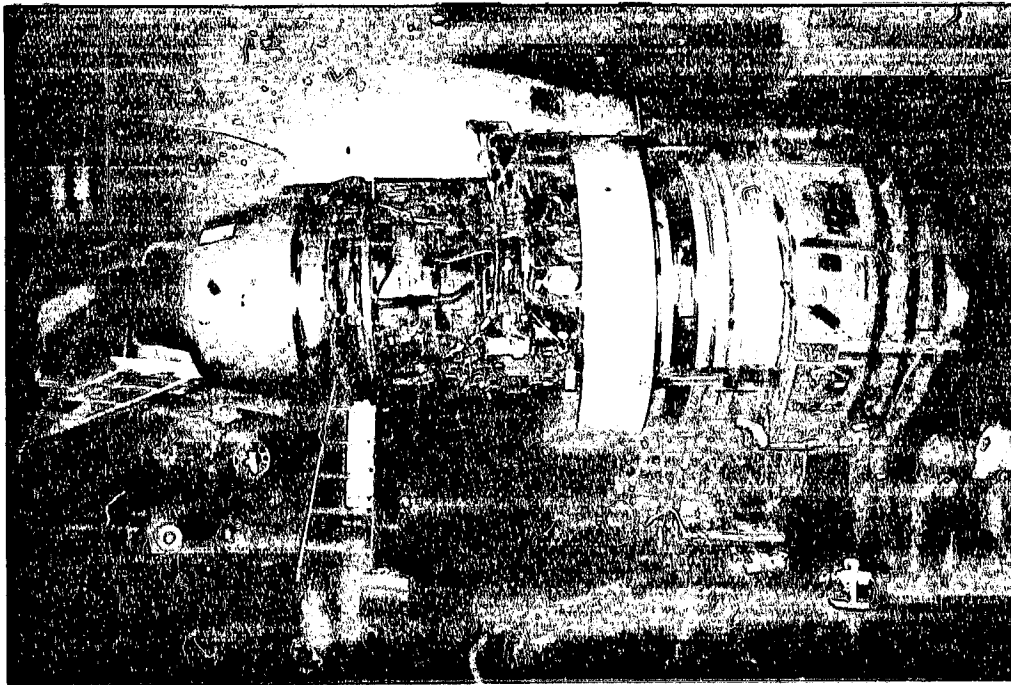
Figure 2-2   Primary Test Engine - The analytically built engine, serial number P-662204, with complete instrumentation was installed on the airplane in position number 3.

(Boeing, FA-122279)

7

A second fan case was analytically built and instrumented with laser clearance monitoring probes. This fan case was installed on the position number 4 engine, and the clearance monitoring instrumentation was connected to the read-out system in the test airplane cabin.

To measure the flight loads simultaneously with the engine data, Boeing, under the Nacelle Aerodynamic and Inertial Loads (NAIL) Program, installed pressure probes around the fan cowls and accelerometers and rate gyroscopes on the engines and mounts. Aerodynamic loads on the two engine inlets were mapped by pressure probes on the position number 3 and 4 engines. Accelerometers on the inlet, fan case, and engine mount struts monitored the inertia loads. Rate gyroscopes on the fan cases monitored the gyroscopic loads. The pressure and acceleration signals were scanned continuously and recorded by the Airborne Data Analysis and Monitoring System. Descriptions of the Boeing Nacelle Aerodynamic and Inertial Loads Program instrumentation and data recording system are presented in the Boeing Test Report for the NAIL Program, Reference 1.

Airplane flight conditions, flight loads, engine performance, turbine case temperatures, and engine running clearances were all recorded along with a time signal to the nearest 0.01 second. Thus, airplane condition, flight loads, and engine response can be compared at any steady state or transient condition.

The position number 3 engine was the primary data source. Lesser instrumentation on the position number 4 engine provided back-up data and the basis for comparing flight loads and engine responses for the inboard and outboard engine installations.

The JT9D Flight Loads Test/NAIL Flight Test Program was conducted by Boeing in October 1980, flying out of Glasgow, Montana. The NASA program included five test flights. However, Boeing concurrently conducted an additional development test program on a new engine installed in position number 2. The additional flights dedicated to and paid for by that program provided significant additional data at no cost to the NASA program.

The flight test program started with the 747 production acceptance test, illustrated in Figure 2-3, since the acceptance test precedes delivery of the airplane to the operator, and data collected in earlier phases of the JT9D Diagnostics Program indicated that a performance loss occurred during the first flight of the airplane. Subsequently, the effects of heavier gross weight take-offs and variation of take-off flap settings were measured. High G turns were performed to simulate the effects of avoidance maneuvers.

8
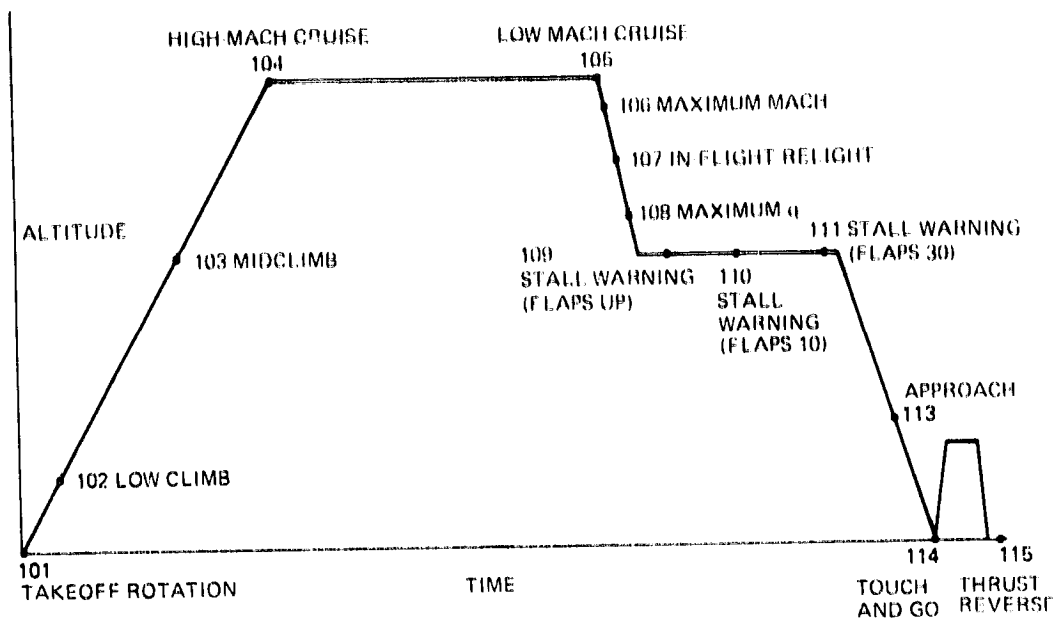
Figure 2-3 Production Acceptance Test Flight Profile - This test pattern was the initial test of the program since it had been indicated that a performance loss occurred on the first airplane flight.

Previous analysis had indicated the possibility of rubs occurring from dynamic loads which could be caused by an extreme air gust condition or a hard landing. No gust conditions were encountered; however, a heavy gross weight, hard landing test was accomplished.

Following completion of the tests, number 3 engine was removed from the airplane and returned to Pratt & Whitney Aircraft where a final calibration test was conducted. The engine was then disassembled, the fan and high-pressure turbine were analytically inspected, and the engine was refurbished and returned to Boeing for use on test airplane RA001.

The actual test sequence was modified slightly from the planned procedure; however, all of the planned test conditions plus some additional conditions were run. The actual ground test calibrations conducted and flight conditions monitored are listed chronologically on Table 2-I.

9

TABLE 2-1

TEST SEQUENCE

Date	Flight Condition Description	Number	Pressure Altitude (feet)	Mach Number	Location
06-24-80	Bare Engine Ground Calibration		Sea Level	0	East Hartford, Conn.
10-03-80	Installed Engine Ground Calibration		Sea Level	0	Boeing Field, Wash.
10-10-80	Installed Engine Ground Calibration		2,560	0	Glasgow, Montana
10-11-80	First Test Flight				Glasgow, Montana
	Acceptance Test Flight:				
	612,000 lb Take-Off with 20 Flaps	101-1	2,560	0.25	
	Mid-Climb	103	17,200	0.60	
	High Mach Number Cruise	104	35,500	0.86	
	Low Mach Number Cruise	105	35,500	0.77	
	In-Flight Relight	107	27,900	0.72	
	Stall Warning with Flaps Up	109	17,000	0.39	
	Stall Warning with 10 Flaps	110	16,200	0.35	
	Stall Warning with 30 Flaps	111	17,000	0.27	
	Idle Descent	112	8,500	0.44	
	Approach	113	6,000	0.27	
	Touch and Go	114	2,560	0.26	
	Thrust Reverse	115	2,560	0.18	
10-11-80	Installed Engine Ground Calibration		2,560	0	Glasgow, Montana
10-19-80	Second Test Flight				Glasgow, Montana
	538,000 lb Take-Off with 10 Flaps	101-2	2,560	0.24	
	Low-Climb	102	5,900	0.39	
	2.0-G Left Turn with Flaps Up	116	8,400	0.49	
	1.6-G Left Turn with 30 Flaps	117	8,200	0.26	
	Airplane Stall	123	9,000	0.21	
10-20-80	Third Test Flight				Glasgow, Montana
	647,000 lb Take-Off with 10 Flaps	101-3	2,560	0.25	
10-20-80	Installed Ground Calibration		2,560	0	Glasgow, Montana
10-25-80	Fourth Test Flight				Glasgow, Montana
	710,000 lb Take-Off with 10 Flaps		2,560	0.25	
	780,000 lb Take-Off with 10 Flaps (Simulated)	118	3,650	0.30	
	690,000 lb Landing				
10-25-80	Fifth Test Flight				Glasgow, Montana
	Maximum Mach Number Flight	106	37,000	0.91	
	Maximum Dynamic Pressure Flight	108	24,500	0.84	
	2.0-G Right Turn with Flaps Up	120	8,200	0.48	
	1.6-G Right Turn with 30 Flaps	121	8,300	0.27	
10-25-80	Installed Ground Calibration		2,560	0	Glasgow, Montana
11-05-80	Installed Ground Calibration		2,560	0	Glasgow, Montana
01-09-81	Bare Engine Ground Calibration, As-Received		Sea Level	0	East Hartford, Conn.
01-12-81	Bare Engine Ground Calibration after Vane Trim		Sea Level	0	East Hartford, Conn.

* Note: A check flight was made on 10-3-80 and a ferry flight was made on 10-6-80. However, both flights were conducted with reduced power on engine number 3 such that no close clearances occurred or were measured.

10

The initial test flight duplicated the acceptance flight with the exception of the maximum Mach number and maximum dynamic pressure cruise conditions. An engine ground calibration and fan inspection were conducted following this initial flight of the test program.

During the second test flight, the acceptance test 10-degree flap setting take-off and climb-out was conducted. High G turns and an airplane stall were also included in this test flight. Rubs were noted on the fan rub strips.

The third test flight included a higher gross weight take-off (647,000 pounds) with flaps set at 10 degrees. Additional fan rub was noted. The third ground calibration followed the flight.

The fourth test flight was conducted with take-off at the highest gross weight that was feasible for the airplane and conditions (710,000 pounds). At 1000 feet above ground, a 1.3-G pull-up was executed to simulate the aerodynamic loads which would occur during a 780,000-pound gross weight take-off to obtain data for the final take-off test condition. The airplane landed with a gross weight of 690,000 pounds at a high sink rate (5 feet/second) in an effort to establish a dynamic load condition. Rubs were noted on the fan rub strips.

The final test flight was then flown to conduct the remaining two acceptance flight conditions (maximum Mach number cruise and maximum dynamic pressure cruise) and the high G turns to the right which were added to the program. The fourth ground calibration followed this flight.

Two additional flights were then conducted to complete the companion test program on the position number 2 engine. Then a final installed calibration was conducted. The airplane was then ferried to Seattle, and the test engine was removed and returned to Pratt & Whitney Aircraft.

The initial bare engine calibration was then repeated at Pratt & Whitney Aircraft in the as-received condition. The fan blades were then washed, the vane trim was checked, and the calibration was repeated.

An analytical teardown and inspection were then conducted on the fan and high-pressure turbine from the primary test engine and the instrumented fan case which was installed on the position number 4 engine.

SECTION 3.0

DATA COLLECTION AND ANALYSIS METHODOLOGY

3.1 LOADS DATA

This category of data includes the flight loads, namely the aerodynamic loads on the fan inlets and the inertial loads. Engine power induced loads which contributed to the clearance closures namely centrifugal, thrust, fan axial and thermal were not measured directly. Their clearance closure effects were either measured or computed.

The aerodynamic loads on the inlets were determined by integrating the measured pressures over the inner and outer surfaces of the inlet (Figure 3-1), giving net shear loads and moments about the fan inlet.

The inertial loads were due to accelerations and gyroscopic effects. Accelerometers and rate gyros were installed on the test engines and supporting structure including the strut-to-wing intersection, and the loads were computed from the recorded acceleration rates.

3.1.1 Data Collection

The aerodynamic loads on the position numbers 3 and 4 engine inlets where determined by continuously measuring the pressures on the inside and outside of those inlets and converting these pressure data into shear loads and bending moments. Reference 1 presents a detailed description of the pressure measurement system. The inboard engine (number 3) was chosen for the more extensive pressure mapping since the aerodynamic load effects were expected to be greater on this engine, Figure 3-1. Fewer pressure taps were installed on the outboard engine (number 4) with sufficient measurements to indicate relative load levels between the inboard and outboard engines.

Instrumentation for intertial loads consisted of accelerometers and rate gyros located on the engine and pylon (Figure 3-2) and the aircraft center of gravity. These instruments were used on both test engines and at their fore and aft wing and pylon interface. For angular accelerations two axes of a three-axis rate gyro mounted on the two test engines were used. Additional accelerometer and rate gyro description is contained in the Flight Loads Test report (Reference 1).

Accelerometers were placed on the engines so that lateral, vertical, and longitudinal accelerations were measured at the positions identified on Figure 3-2. Rate gyros were placed at 3 o'clock in the fan case and were used to measure pitch and yaw rate. A total of six accelerometers and one rate gyro per engine permitted calculation of the translational and angular accelerations at the engine center of gravity.
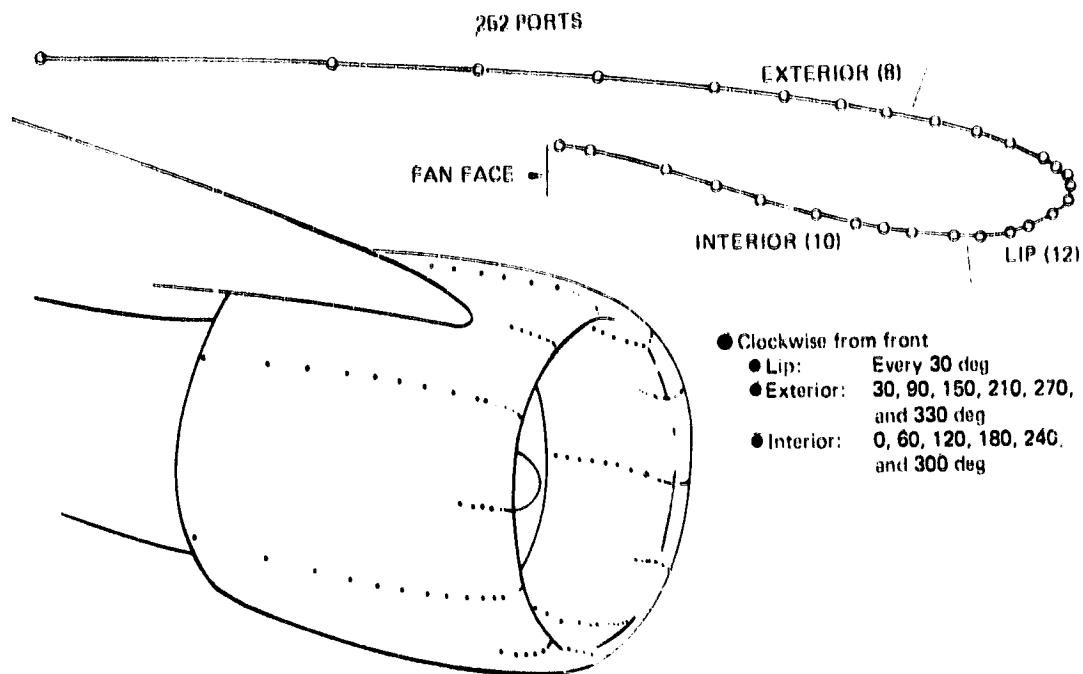
Figure 3-1   Inboard Inlet Pressure Taps

Accelerations were measured at the pylon/wing interfaces. The lateral accelerations were measured at the wing front spar and rear thrust link attach point (Figure 3-2). The vertical accelerations were measured inboard and outboard of the front spar attach point and on the rear thrust link attach point. In the longitudinal direction, accelerations were measured only at the front spar. Each interface had a total of six linear accelerometers.

Basic airplane information was recorded, including pitch, yaw, and roll angles along with side-slip and angle of attack. Angular accelerations about all three axes were measured at the aircraft center of gravity.

ACCELEROMETERS   PITCH AND YAW RATE GYROS NEAR FAN FACE

● Inboard and outboard engines

SIX NEAR
STRUT ATTACH
POINTS

FRONT
SPAR

FOUR NEAR
FAN FACE

TWO NEAR
INLET TIP
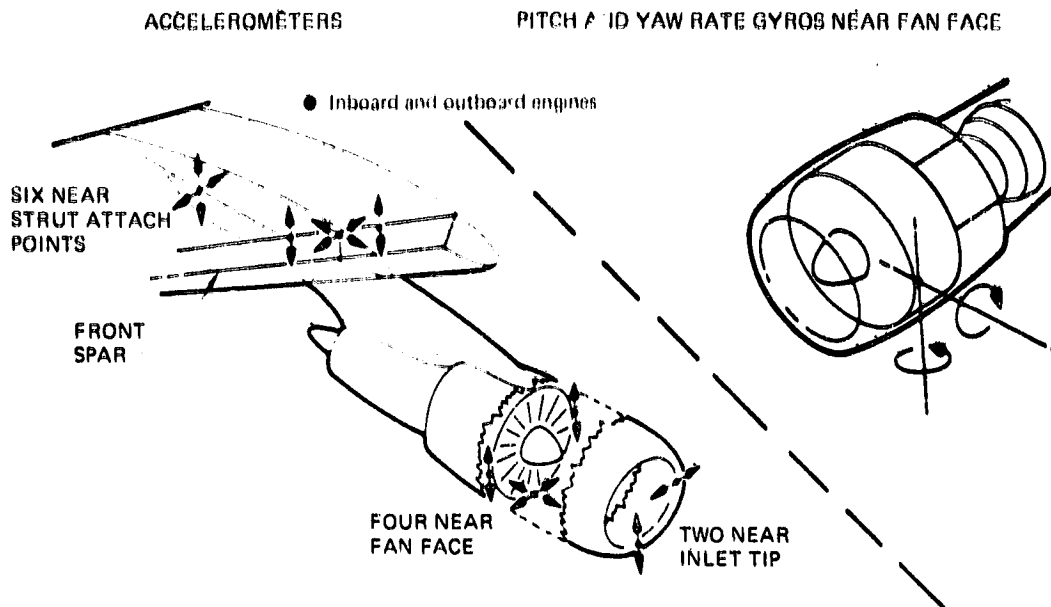
Figure 3-2   Inertial Data Sensors

3.1.2   Analysis of Loads Data

The pressure readings taken from the 252 ports on the position number 3 engine and the 45 ports on the number 4 engine were integrated using a Fourier-Bessel interpolation in the circumferential direction and a linear interpolation in the axial direction.

The axial pressure distributions for each of the selected flight conditions were determined and plotted graphically, examples of which are shown in Figures 3-3 and 3-4. The pressures are plotted in terms of pressure coefficient versus nominal arc lengths. Each flight condition is covered by two plots, one (inlet pressures) pertaining to the rows of pressure ports that extend all the way into the inlet (i.e., θ = 0 degree, 60 degrees) and the other (cowl pressures) pertaining to the rows that extend to the trailing edge of the fan cowl (i.e., θ = 30 degrees, 90 degrees).
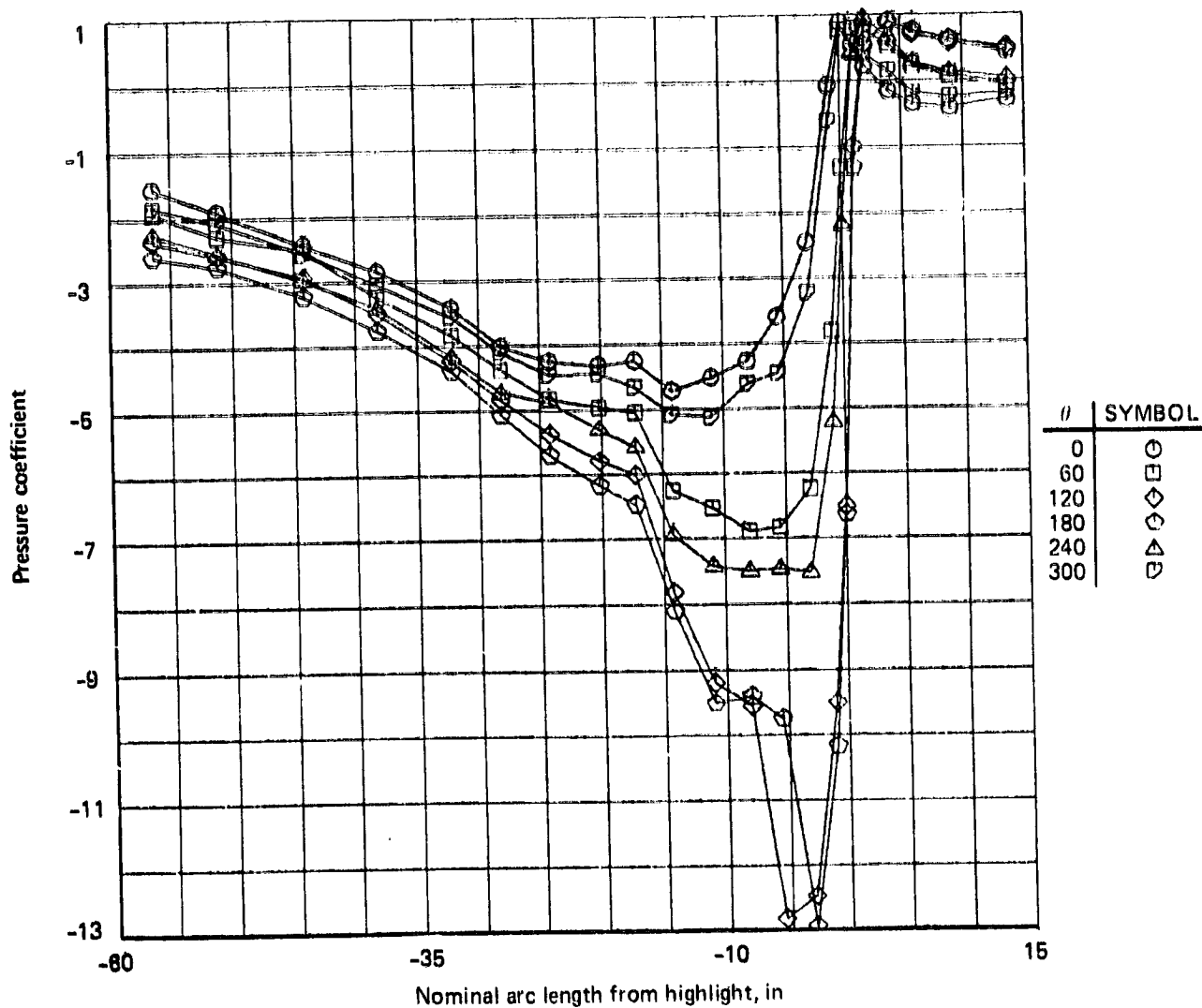
Figure 3-3 Engine Number 3 Inlet Pressures; Condition 101, 612,000-pound Gross Weight Take-Off with 20-degree Flaps
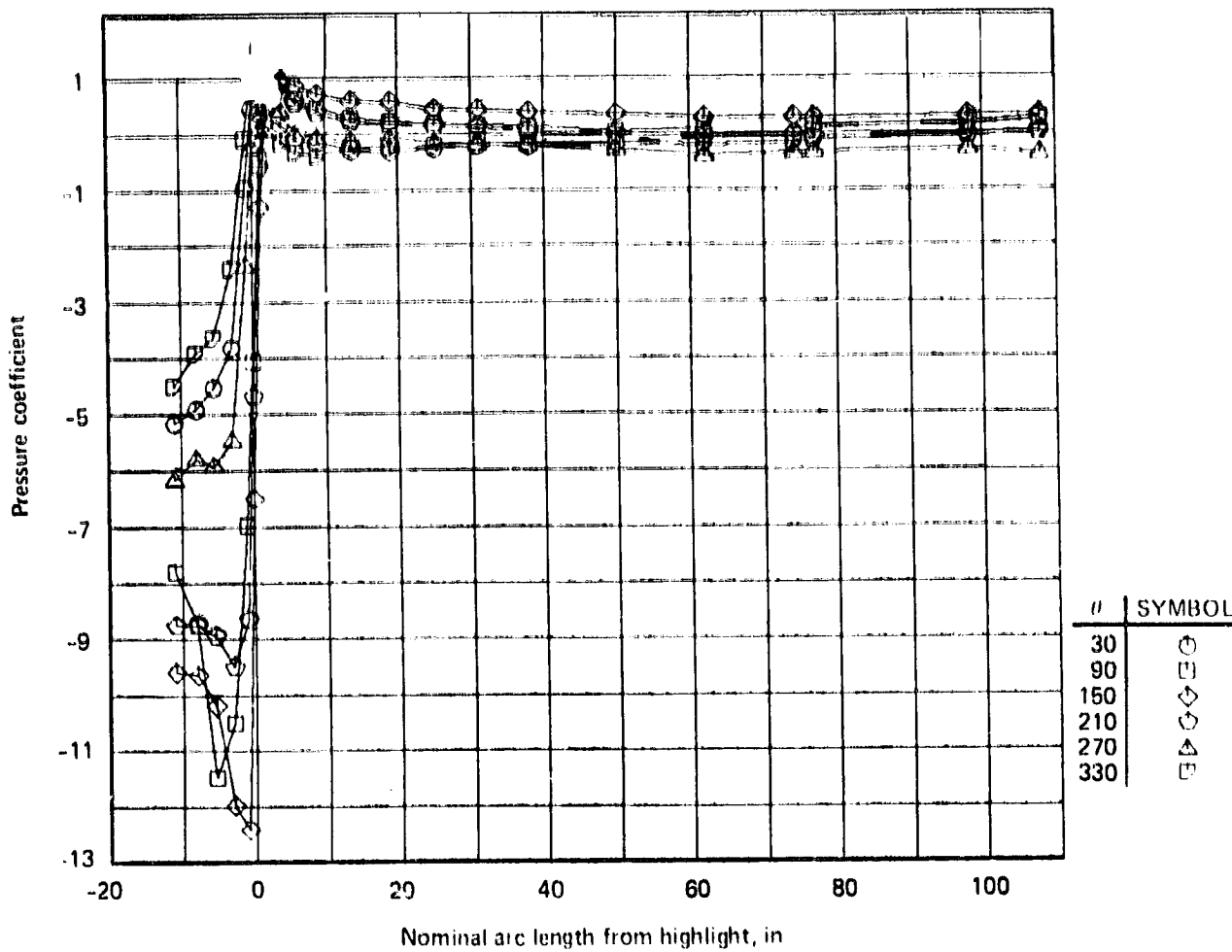
Figure 3-4 Engine Number 3 Cowl Pressures; Condition 101, 612,000-pound Gross Weight Take-Off with 20-degree Flaps

17

To compute resultant air loads from the pressure data, a previously developed computer program was used. It approximates the inlet and cowl geometry as a series of conical frustums and adjusts for the tilt of the axis with respect to the nacelle centerline by insertion of wedge-shaped surfaces. Figure 3-5 shows the coordinate system for the resultant loads. [Note that the resultant shear loads and moments are all referenced to the "A" flange (the fan-to-inlet interface). The moment at the engine front mount, at the rear of the fan case, di to the aerodynamic load is about 50 percent greater than at the A" flange.] This procedure was checked by comparison to a method based on a complete three-dimensional geometry definition. Resultant forces differed by less than three percent, and resultant yaw and pitching moments at the engine face differed by less than 1 percent. (Rolling moments differed by 3.5 percent but are not significant loads.)
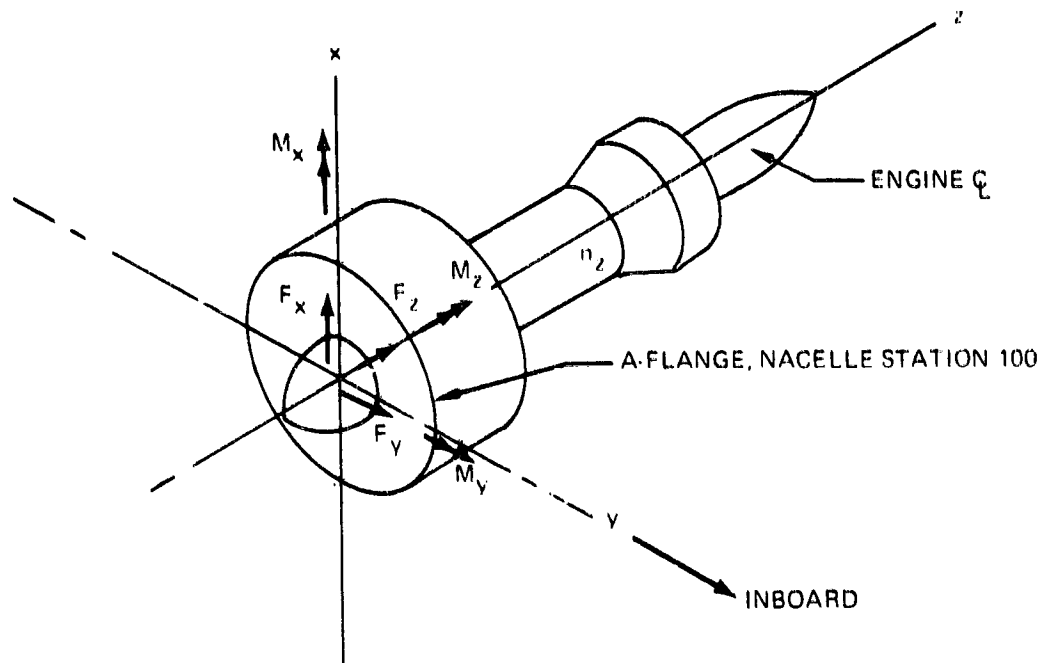
Figure 3-5   Sign Convention for Steady-State Loads, Engine Number 3

Pitch and yaw rates as well as accelerations were recorded throughout all test flights. The data was plotted in graphical form for the selected flight condition time frames. Figure 3-6 shows the normal accelerations at the aircraft center-of-gravity during the hard landing at the end of the fourth flight and is typical of these plots. Engine acceleration data were filtered to pass frequencies below 40 Hertz (Hz). Pitch and yaw rates were filtered to pass frequencies below 5 Hertz.

18
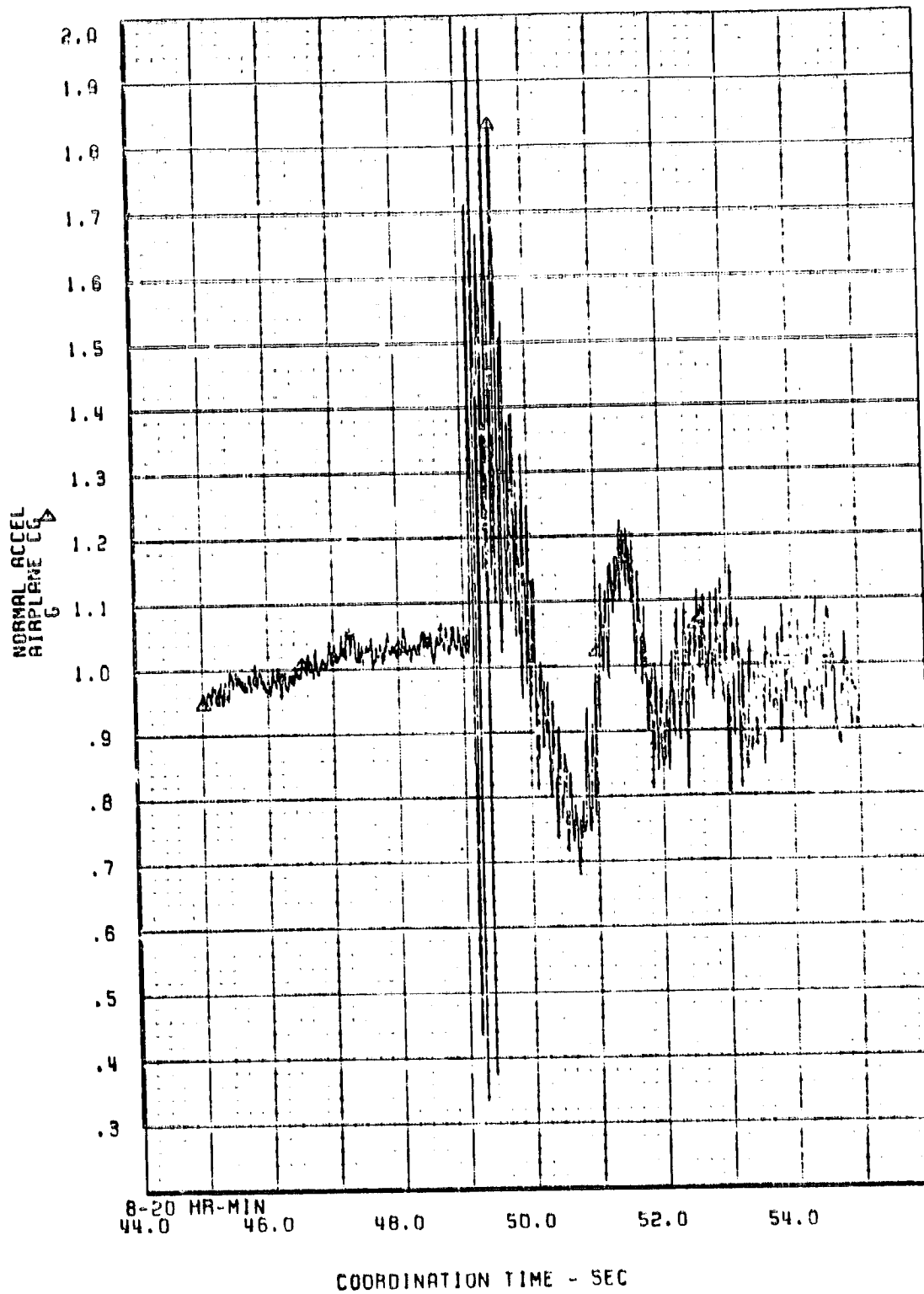
Figure 3-6 Airplane Center-of-Gravity Normal Acceleration During the Hard Landing

The six accelerometers in the nacelle measured linear accelerations. The measurements were used to determine the six components (three linear and three angular) of accelerations at the center of gravity.

Assuming a rigid body motion of the nacelle, the measured accelerations (a) are related to the engine center-of-gravity acceleration (A) by:

$$(a) = [B] \ (A) \tag{1}$$

where [B] is a six-by-six transformation matrix that depends upon the location of the instrumentation in the nacelle. The equation

$$(A) = [B]^{-1} \ (a) \tag{2}$$

provides the history (A) based on the measured time history of (a). In this manner (A), whose components are A_x, A_y, A_z, ϕ, θ, and ψ, was determined and the values obtained for each time point of interest for either comparison with previous predictions or use in further analysis using the finite element model of the 747/JT9D propulsion system.

The preparation of finite element grid point forces for subsequent structural modeling was accomplished by integrating pressures over the aerodynamic surface mesh, then transforming the mesh forces to the structural surface representative of the finite element mesh.

G loads were generated by applying an inertia load factor to the finite element mass matrix to generate grid point inertia forces.

Gyro moments for each rotor grid point were generated by multiplying the pitch or yaw rate by one-half the grid point transverse mass moment of inertia times the rotor speed.

3.2 CLEARANCE CLOSURE DATA

Running clearances of the fans in both engines and of the first turbine stage in the position three engine were monitored throughout the flight testing and the installed ground calibration testing using a laser probe system developed for the prior Simulated Aerodynamic Loads Test program. Measured clearances, exact time, and engine speed were recorded on video tape for subsequent analytical comparison with flight loads and other recorded test parameters.

High pressure turbine case temperatures on the number three engine were also monitored continuously to provide transient and steady state thermal effect data for use in the analysis of clearance changes in the turbine.

20

3.2.1 Data Collection

Twelve laser probes were installed on the two engines. Four were mounted to measure fan blade/outer air-seal running clearances in the outboard engine. The locations are shown on Figure 3-7. The inboard engine was equipped with four similarly mounted fan clearance probes plus four probes to measure first-stage high-pressure turbine blade running clearance. The turbine probe locations are shown on Figure 3-8. There were some limitations on probe location; hence, the selected positions were as shown on Figure 3-7 and 3-8. Bottom dead center (±10 degrees) was avoided due to the possible build-up of contaminants that would blind the probes.

REAR VIEW LOOKING FORWARD
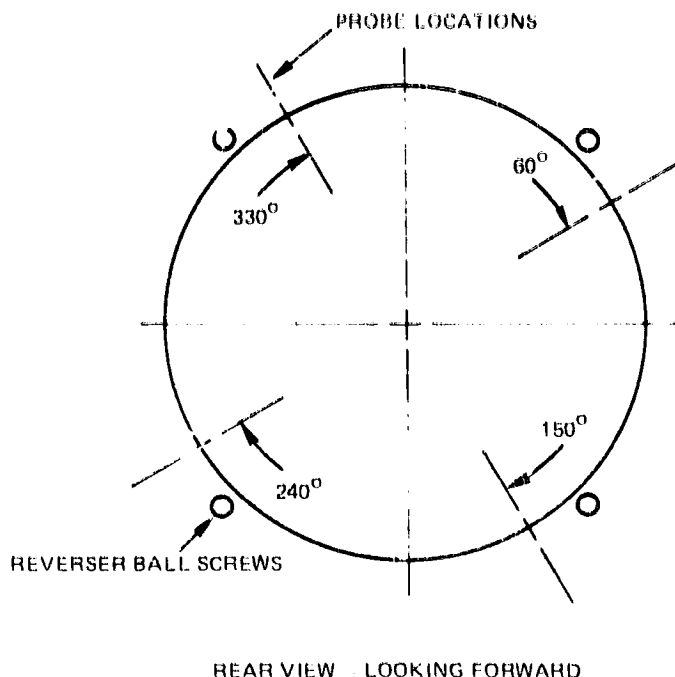
Figure 3-7 Angular Location of Fan Blade Laser Proximity Probes - Four probes, located 90 degrees apart, provided adequate clearance monitoring data.

The four clearances measured by the laser probes in each of the three probe systems as well as engine speed and time were recorded continually on video tape every 1/30 of a second for subsequent transient and steady state analysis and comparison with loads. A description of the laser clearance monitoring system and its operation is included in Reference 2.

PROBE LOCATIONS

ENGINE MOUNT FRAME

CIRCUMFERENTIAL TUBING (REROUTED)

PRE COOLER

338°

60°

NO. 3 BREATHER LINE

8TH BLEED PIPE

142°

232°

TUBES

STARTER BLEED

HEAT SHIELD

REAR VIEW - LOOKING FORWARD
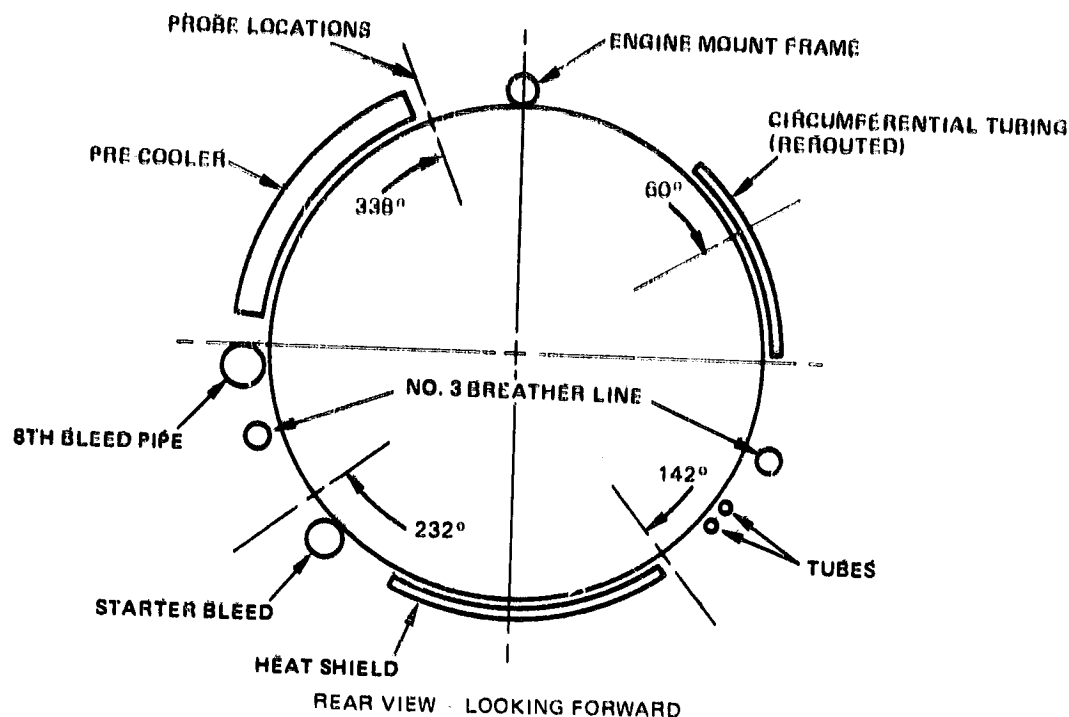
Figure 3-8 Angular Location of High-Pressure Turbine Blade Laser Proximity Probes - Four probes, located approximately 90 degrees apart, provided adequate clearance monitoring data.

The major temperature excursions and corresponding influences on the JT9D engine blade tip clearances occur in the high-pressure compressor, high-pressure turbine, and low-pressure turbine with the largest influence in the high-pressure turbine. Transient and steady state turbine running clearances are influenced by: 1) centrifugal force and temperature-induced disk and blade growth; 2) temperature and aerodynamic load-induced case growth and deflection; and 3) by thrust and inertia load-induced rotor movement. The laser probes measured the total running clearance change. Simultaneous monitoring and analysis of the high-pressure turbine case temperatures during flight and ground testing provided a better understanding of case growth and its influence on running clearances.

Radial, axial, and circumferential temperature patterns in the high-pressure turbine case of the position number 3 engine, under steady state and transient conditions, were established by 18 thermocouples installed around the turbine case front and rear (M and N) flanges plus two thermocouples mounted in the air space above and below the case, as shown in Figure 3-9. These temperatures were continuously recorded on the two Boeing ADAMS systems which provided transient and steady-state data and time sychronization for subsequent analysis.

22
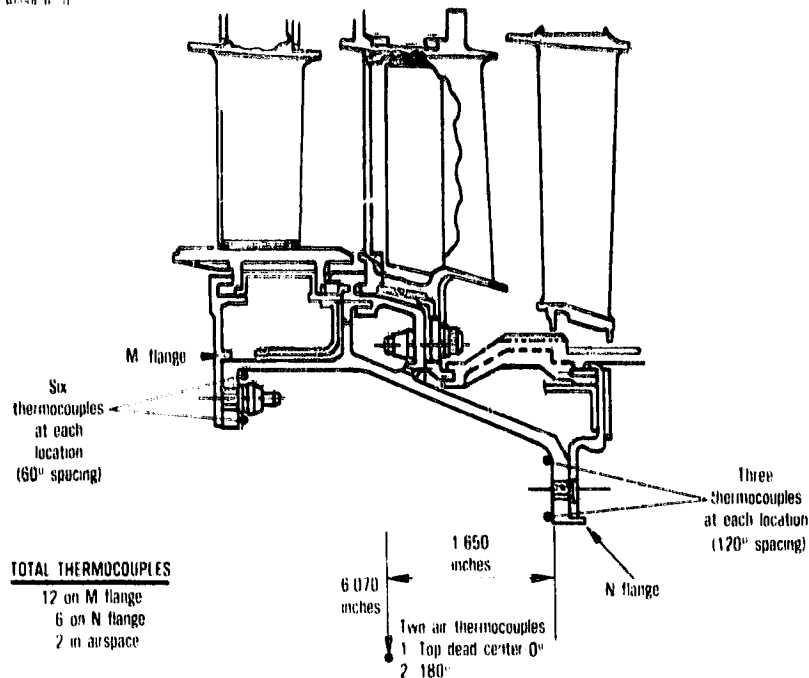
Figure 3-9 High-Pressure Turbine Case Thermocouple Locations - All
circumferential locations are measured clockwise, looking
forward. (J24018-24)

3.2.2 Analyses of Clearance Data

Clearances and case temperatures were measured and recorded throughout
the flight tests and ground calibrations. A reference set of
clearances was established based on the recorded clearances at
stabilized ground idle power level immediately prior to the first test
flight. Subsequent clearance closures at conditions of interest were
then defined by correcting the measured values to these reference
values. The analytical interpretation of these measured blade-to-case
closures can be described as the combination of engine power-induced
effects and flight load effects.

Engine power-induced closure is the result of:

o Blade and disk axisymmetric growth caused by power-induced
   centrifugal and thermal loads,

o Case axisymmetric and asymmetric growth caused by power-induced
   thermal expansions of rotating and static components, and

o Thrust-induced asymmetric bending of the engine.

23

Flight load-induced closure is the result of:

o Asymmetric bending of the engine due to aerodynamic loads on the inlet cowl,

o Gravitational (G) loads and gyroscopic (gyro) loads associated with airplane maneuvers, and

o Dynamic vibration induced closures.

The laser system measured the total clearance change at each probe at an instant in time. This closure is the algebraic sum of the above effects which were acting at the time of measurement. Separating these effects was accomplished by using various combinations of measured data and previously developed structural and thermal analytical models. As an example, total axisymmetric closure was determined from the average of the four closure readings. Centrifugal force induced axisymmetric closure was computed knowing rotating hardware characteristics and was checked by measuring the instantaneous total axisymmetric closure change coincident with a fast acceleration or deceleration. Aerodynamic load effect was calculated using finite element analysis techniques and measured aerodynamic loads and was checked by comparing measured closures immediately preceding and following take-off rotation.

The power-induced axisymmetric closure was measured both on the ground and at altitude for different stabilized engine speeds. It was necessary to measure these closures at both conditions since fan clearance was significantly less at altitude as a result of reduced gas bending loads on the blades.

The axisymmetric closure at a particular time in the flight cycle, together with the cold build clearance, defined the gaps available for the accommodation of additional deflection due to external flight loads.

Axisymmetric and asymmetric closures were evaluated for each flight condition; however, only the maximum closures that contributed to engine deterioration were fully explored.

The asymmetric closure due to thrust and flight load-induced engine bending was isolated using the NASTRAN (NASA STRuctural ANalysis) finite element mathematical model of the JT9D/747 propulsion system with the measured loads and calculated thrust levels as input. The mathematical model was jointly developed by Pratt & Whitney Aircraft and Boeing and began with an identification of below-the-wing propulsion system substructures which were provided by each party. Since primary emphasis in the study was on behavior of the engine, the wing was not included. By excluding the wing, the nacelle/strut combination could reasonably be assumed to be symmetric about a vertical plane through the engine centerline, and the engine behavior could then be calculated with a half model for much less cost than for a full model.

24

Substructure interfaces were chosen where subassemblies were mechanically joined (that is, mount points, flanges, etc.). Detailed finite-element models of the engine static structure (cases and bearing support frames), rotors, and thrust yoke were provided by Pratt & Whitney Aircraft. Rotors were modeled as beams with discrete masses input directly. Boeing provided the inlet, strut, and tail-cone models.

Secondary structural components (fan and core cowls, fan and turbine reversers, stator assemblies), accessories, and plumbing were included as discrete or distributed masses as appropriate to bring the mass properties of the model to within 5 percent of the actual hardware. The final static model consisted of eight substructures with approximately 11,000 degrees of freedom, as shown in Figure 3-10.
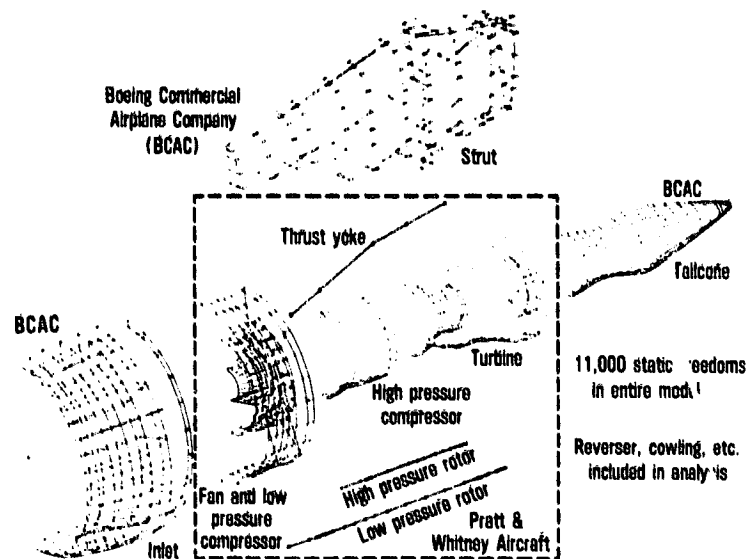
Figure 3-10   JT9D/747   Integrated   NASTRAN   Finite   Element   Structural Model - The model consists of eight substructures with approximately 11,000 degrees of freedom.   (J20152-9)

The flight acceptance profile incorporated in the model includes the proper combination of measured nacelle loadings, engine thrust, inertia and gyroscopic effects, base-line clearances, and air-seal/blade abradability factors. Exposure to thrust and maneuver loads results in deformation of propulsion system structural members and leads to relative motion between static and rotating components of flow-path seals. If the motions are larger than can be accommodated by the available clearances, rubs and wear (air-seal/blade tip rubbing) will occur and result in increased operating clearances between blade tips and outer air seals. Abradability factors determine the trade-off between blade tip and outer seal wear. Performance influence coefficients for each engine stage are then used to determine the performance loss due to these increased operating clearances.

High-pressure turbine case metal temperatures at the front and rear flanges, shown previously in Figure 3-9, were recorded simultaneously with performance and clearance parameters during each of the test conditions. The case temperature data were recorded on the Boeing Airborne Data Analysis and Monitoring System (ADAMS). The data tapes were then processed by Pratt & Whitney Aircraft to define transient and steady state temperature patterns in the radial, axial, and circumferential directions.

Analytical models for predicting the steady state and transient thermal growth characteristics of the turbine assembly were validated and, where necessary, corrected using the case temperature, gas temperature, and directly-measured clearance data. Turbine case thermal expansion response rate to thermal transients was found to be faster than predicted by the analytical models, which were subsequently revised. The revised models were then used in the analysis to establish and quantify the various causes of clearance closure at the critical ground test and flight conditions.

3.3 PERFORMANCE DATA

Expanded performance instrumentation was installed on the instrumented inboard engine during the preprogram and postprogram bare engine calibrations at the Pratt & Whitney Aircraft Middletown (Connecticut) test facility and throughout the ground and flight testing with that engine installed on the airplane. The engine used in the flight program was equipped with expanded instrumentation sensors as described below in this section.

The engine performance instrumentation used in the bare engine calibration and in the flight test program is listed on Table 3-I. The measurements in the test stand and on the airplane are essentially the same with the principle difference being that thrust is directly measured in the test stand but not on the airplane.

When the engine was installed in the test airplane the engine performance instrumentation was readout and recorded by the ADAMS system thus providing a simultaneous recording on clearance, flight loads, engine performance and airplane flight condition data.

A preflight performance calibration of the newly assembled engine was made in the Pratt & Whitney Aircraft test facility in Middletown, Connecticut. After the engine was installed in the number 3 position on the airplane, a five-point installed base-line ground calibration was conducted at Boeing Field, Washington. This base-line calibration was repeated after a functional check flight and the ferry flight to Glasgow, Montana when it was learned that air was inadvertently being bled from the engine during the original installed calibration. Each of the subsequent test flights was followed by a ground calibration. Upon completion of the NAIL program flight testing, several additional

26

TABLE 3-I

PERFORMANCE TEST INSTRUMENTATION

Parameter	No. of Probes	No. of Measurements	When Used In Test Cell	When Used Installed On Airplane
Pamb	-	1	x	x
Pt1	1	1		x
Pt2	8	8	x	
Pt2, Ps2	8	8	x	
Pt2.5	6	1	x	x
Pt3	3	1	x	x
Ps3	3	1	x	x
Ps4	1	1	x	x
Ps5i	1	1	x	
Pt7	6	1	x	x
Pcell fan	8	1	x	
Pcell primary	4	1	x	
Tamb	-	1	x	x
Tt2	8	8	x	
Tt3	1	1	x	x
Tt4.5	3	1	x	x
Tt6	6	7	x	x
Tt7	6	7	x	x
Tf	-	1	x	x
Specific humidity	-	1	x	
Thrust	-	1	x	
Wf	-	2	x	x
N1	-	1	x	x
N2	-	1	x	x
Vane Angle (β)	-	1	x	
EVC	-	1	x	x
Condition Lever Angle	-	1	x	
Bleed Valve Positions	-		x	x
Cross feed Valve	-	1		x
Precooler Exit Valve	-	1		x

flights were made for the JT9D-7R4 engine development program being conducted in conjunction with the NAIL program. Then a final installed calibration of the NAIL engine was conducted prior to the ferry flight back to Boeing Field and removal of the engine. Two postflight performance calibrations were conducted in the Middletown test facility, one in the as-received condition and a second calibration after a vane trim check and fan blade wash. See Table 2-I.

Build clearances were measured in the rebuilt fans and high-pressure turbine prior to the start of testing. Rub depths were measured around the airseals of the two fans after each ground calibration and test flight. Finally, an analytical teardown of the fan and high-pressure turbine of the number 3 test engine were conducted after the test program to identify the magnitude and location of all blade and seal wear in these new components.

SECTION 4.0

RESULTS

4.1 MEASURED LOADS

4.1.1 Steady cr Quasi-Steady Loads

Table 4-I gives the resultant air loads along with key aircraft parameters for 23 flight conditions selected for analysis. Note that pitching and yaw moments are about the "A" flange (the fan-to-inlet interface). The moment about the engine front mount is approximately 50 percent greater.

Four take-offs [one with 20-degree flaps and a 612,000-pound gross weight and three with 10-degree flaps and gross weights of 538,000, 647,000, and 780,000 pounds (simulated)] were selected for detailed loads analyses. Time histories of resultant loads were calculated for the purpose of correlating maximum clearance changes, whenever they occurred, with the aerodynamic loads. For the 780,000-pound take-off, which was simulated by a pull-up maneuver at 1,000 feet above ground level, data for the analysis were recorded when the correct airplane lift coefficient was reached.

The 612,000-pound gross weight take-off with 20-degree flaps (condition 101-1) was the initial take-off for the entire test program (see Table 2-I). Peak load was reached at seven seconds after rotation. The pitching moment at the A-flange was 329,000 inch-pounds.

The 538,000-pound take-off with 10-degree flaps (condition 101-2) was the acceptance test flight take-off. Note that while the gross weight, air speed, and fan flow rate were all less than for the first take-off, the pitching moment of 401,000 inch-pounds was 22 percent greater than that for the first take-off. This difference in pitching moment was due to the greater rotation angle required with the lower flap setting to achieve required lift for take-off. The measured "airflow vane angles" on the right and left sides of the cabin reflect the variations in the inlet angle of attack, Figure 4-1. These angles are plotted on Figure 4-2 for the take-off condition along with the pitching moment. Note that in this ten second period of near constant ground speed and engine speed, the pitching moment appears directly proportional to the change in vane angle with the peak again occurring about seven seconds after start of take-off rotation.

The third take-off was executed at 647,000 pounds gross weight and 10-degree flaps (condition 101-3). Although flap and power settings were the same, the aerodynamic loads, Figure 4-3, were greater than those for the second take-off because of higher air speed at lift-off. (Note, however, that the increase is less than proportional to the increase in gross weight.)

TABLE 4-I

AERODYNAMIC LOADS ON ENGINE NUMBER 3

Condition	Calibrated airspeed km/h	(kcas)	Referred airflow, kg/s	(lb/s)	Load factor, g	F_x N	(lb)	F_y N	(lb)	M_x* N·m	(in-lb)	M_y* N·m	(in-lb)
101-1 Takeoff 612 000 lb GW (flaps 20)	292.4	(157.8)	702.6	(1 549)	1.14	26 694	(6 001)	-12 250	(-2 754)	-16 692	(-147 735)	-37 348	(-328 750)
101-2 Takeoff 538 000 lb GW (flaps 10)	279.8	(151.0)	692.6	(1 527)	1.26	32 012	(7 197)	-12 970	(-2 916)	-17 207	(-152 232)	-45 260	(-400 756)
101-3 Takeoff 647 000 lb GW (flaps 10)	296.7	(160.1)	691.3	(1 524)	1.17	35 233	(7 921)	-13 842	(-3 112)	-18 002	(-159 325)	-48 018	(-424 587)
118 Simulated takeoff 780 000 lb GW (flaps 10)	340.2	(183.6)	713.5	(1 573)	1.20	37 114	(8 344)	-12 263	(-2 757)	-15 145	(-134 045)	-48 602	(-430 154)
102 Low climb	405.5	(218.8)	698.1	(1 539)		20 777	(4 670)	-4 746	(-1 067)	-5 125	(-45 361)	-23 260	(-206 045)
103 Mid climb	538.2	(290.4)	735.7	(1 622)		18 166	(4 084)	-2 615	(-588)	-2 910	(-25 758)	-14 224	(-125 891)
104 High M cruise	539.8	(291.3)	740.7	(1 633)		10 982	(2 469)	-4 551	(-1 023)	-4 103	(-36 317)	-6 716	(-59 441)
105 Low M Cruise	478.7	(258.3)	727.6	(1 604)		15 470	(3 478)	-5 031	(-1 131)	-4 772	(-42 237)	-11 994	(-105 150)
106 Max M	554.1	(299.0)	744.8	(1 642)		1 343	(302)	-2 064	(-464)	-1 783	(-15 779)	2 183	(19 317)
107 Inflight relight	529.5	(285.7)	619.2	(1 365)		14 576	(3 277)	-3 274	(-736)	-2 897	(-25 639)	-9 587	(-84 847)
108 Maximum q	662.5	(357.5)	733.5	(1 617)		-6 272	(-1 410)	4 377	(984)	3 282	(29 060)	11 319	(155 411)
109 Stall warning (flaps up)	349.1	(188.4)	721.7	(1 591)		24 184	(5 437)	-6 156	(-1 384)	-7 206	(-63 775)	-27 480	(-243 214)
110 Stall warning (flaps 10)	313.6	(169.2)	735.3	(1 621)		27 707	(6 229)	-9 528	(-2 142)	-10 962	(-97 024)	-34 435	(-304 770)
111 Stall warning (flaps 30)	239.6	(129.3)	740.7	(1 633)		17 467	(3 927)	-5 747	(-1 292)	-8 236	(-72 893)	-24 940	(-220 730)
112 Idle descent	462.7	(249.7)	339.3	(748)		18 370	(4 130)	-5 080	(-1 124)	-3 352	(-29 669)	-10 986	(-97 234)
113 Approach	291.7	(157.4)	701.7	(1 547)		16 489	(3 707)	-6 276	(-1 411)	-8 091	(-71 607)	-22 807	(-201 854)
114 Touch and go	308.6	(166.5)	720.8	(1 589)		19 518	(4 388)	-10 324	(-2 321)	-14 194	(-125 622)	-27 304	(-241 654)
115 Thrust reverse	209.8	(113.2)	621.0	(1 369)		196	(44)	-144	(-10)	-1 954	(-17 259)	-4 528	(-40 363)
116 2.0g left turn (flaps up)	514.3	(277.5)	708.5	(1 562)	1.99	32 079	(7 212)	-15 386	(-3 459)	-15 060	(-133 292)	-29 850	(-264 196)
117 1.6g left turn (flaps 30)	265.0	(143.0)	698.1	(1 539)	1.61	23 543	(5 293)	-16 333	(-3 672)	-21 605	(-191 227)	-32 151	(-284 557)
120 2.0g right turn (flap up)	504.3	(272.1)	542.5	(1 196)	2.04	33 956	(7 634)	-7 246	(-1 629)	-5 362	(-47 455)	-27 058	(-239 481)
121 1.6g right turn (flaps 30)	280.4	(151.3)	650.9	(1 435)	1.60	24 090	(5 416)	-1 597	(-359)	-1 142	(-10 105)	-31 865	(-282 023)
123 Airplane stall	214.4	(115.7)	703.5	(1 551)		27 004	(6 072)	-7 175	(-1 613)	-10 076	(-89 181)	-41 445	(-356 819)

* At "A" Flange
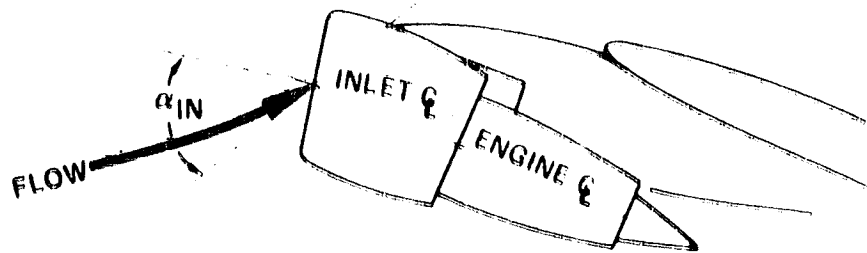
Figure 4-1 Inlet Angle of Attack - The inlet angle of attack (α) is
defined as the angle between the inlet centerline and the
local relative wind that would prevail if the
engine/nacelle/inlet were not present.

The simulated high gross weight take-off (condition 118) was conducted
during the fourth test flight. The actual gross weight was 696,500
pounds. The simulation was achieved by performing a pull-up, starting
at 185 knots and 3646 feet pressure altitude (about 1000 feet above
actual ground) to produce the same airplane lift coefficient that would
occur during a 780,000-pound take-off. The moment at the A-flange was
430,100 inch-pounds.

Figure 4-4 presents a plot of pitching moment versus take-off gross
weight for the four test take-offs. The benefit of the reduced
aerodynamic load with the 20-degree flap setting is obvious.

As seen on Table 4-I, the take-off conditions provide the maximum
aerodynamic loads for normal revenue service (conditions 101, 102
through 105, 113, and 115) and for the acceptance test flight
(conditions 101-2 and 102 through 115). However, three other
conditions are of interest because of possible adverse combinations of
aerodynamic loads and thermal transients in the engine. Figure 4-5
shows a time history of the pitching moment at the engine face, engine
airflow, and body vane angle for condition 110 (stall warning with
10-degree flaps). The maximum moment (305,000 inch-pounds) coincided
with maximum engine airflow, although the maximum vane angle occurred
earlier in the maneuver. The result shows the sensitivity of
aerodynamic loads to fan inlet airflow as well as to inlet angle of
attack and air speed.

The second conditions of interest are the left and right high-G turns
(conditions 116, 117, 120 and 121). The left turns combined high angle
of attack and high airflow with resultant high aerodynamic loads. The
right turns were executed at a lower power level (fan airflow). The
resultant loads were comparable in the vertical axis (Fx and My) but
lower in the lateral axis (Fy and Mx).
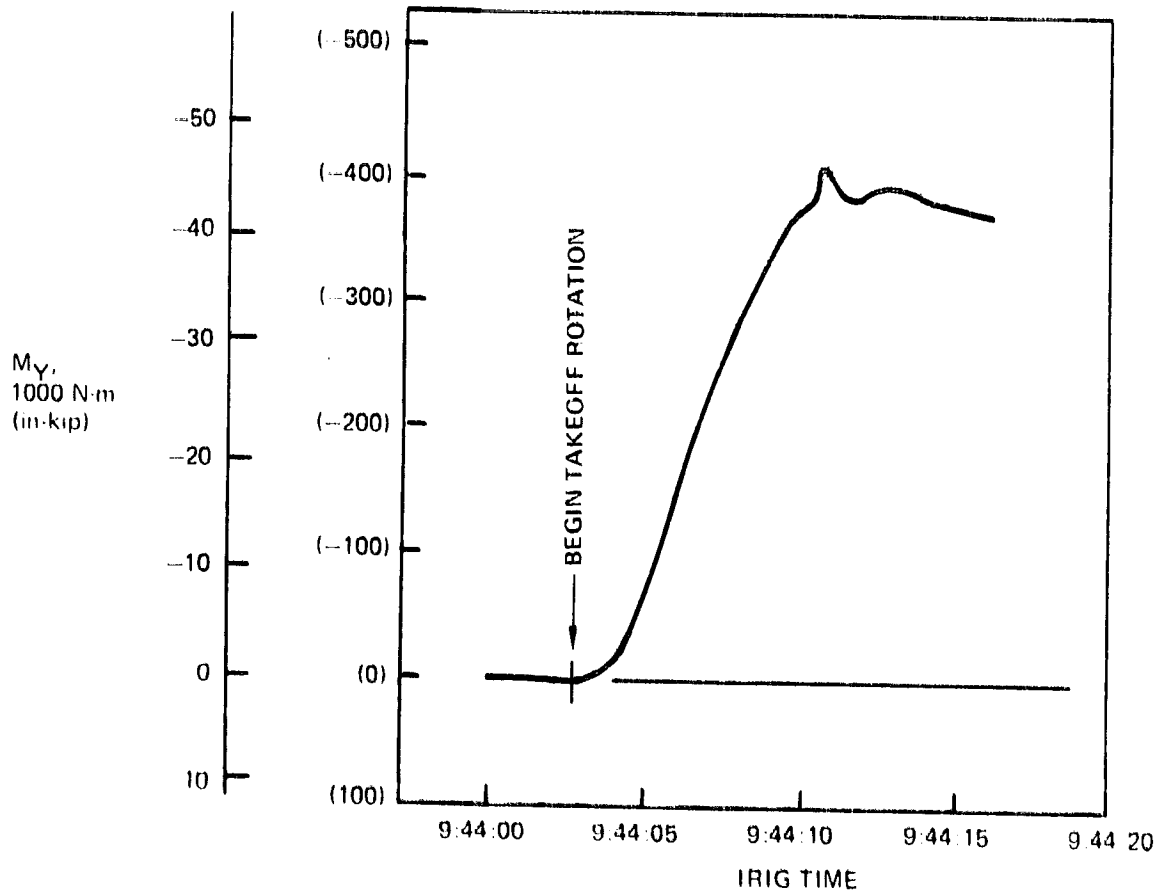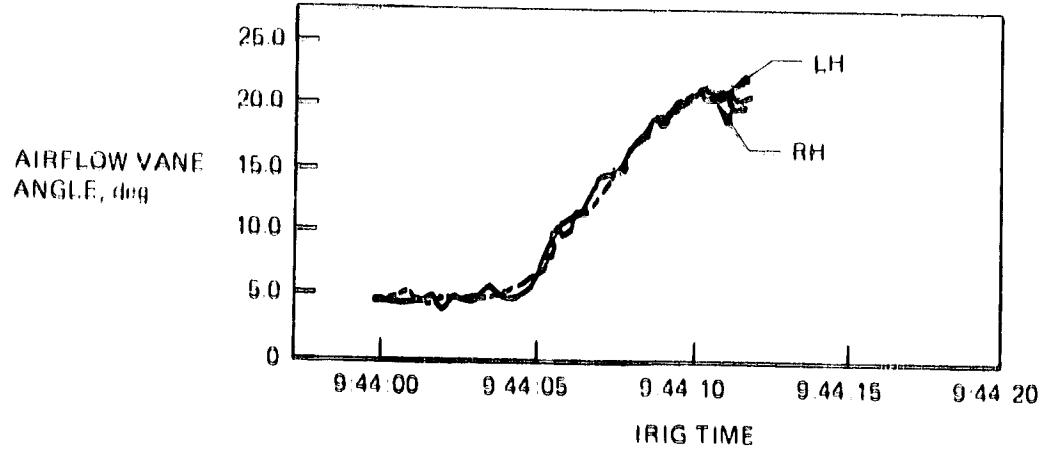
Figure 4-2 Inlet Pitching Moment Time History for the 538,000-pound Gross Weight Take-Off

The third condition of interest was the airplane stall (condition 123) which occurred during the second test flight. The moment peaked at 367,000 inch-pounds. This relatively high load level resulted from a very high angle of attack. The pitch and yaw rates were both about 5.5 degrees per second, and the g level was 1.27. These factors in combination made it an interesting case to examine in detail.

Review of the test data indicated that the measured aerodynamic pressures on engine number four were very close to the pressures of engine 3, implying that the flight loads were about equal.
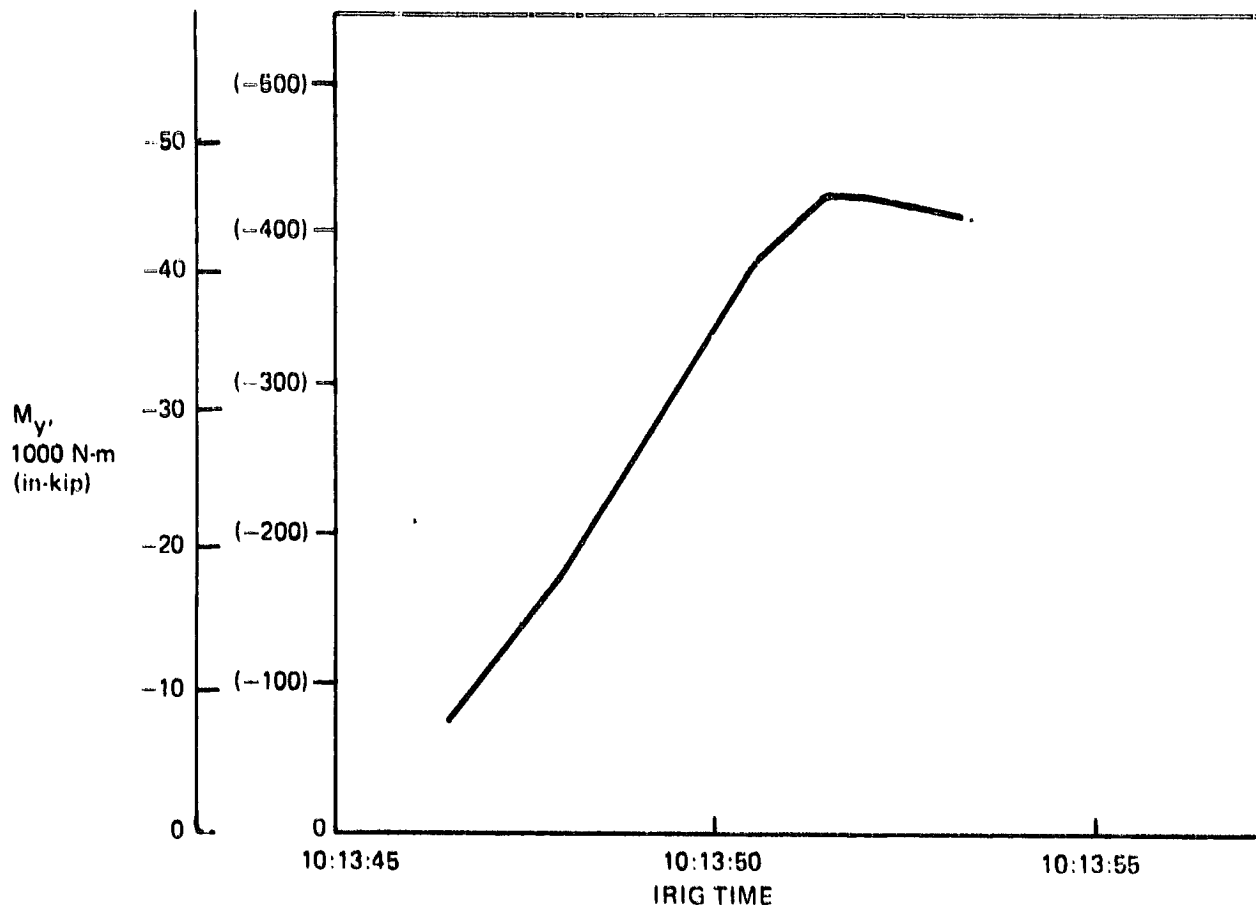
Figure 4-3   Inlet Air Load Moment Time History for the 647,000-pound Gross Weight Take-Off
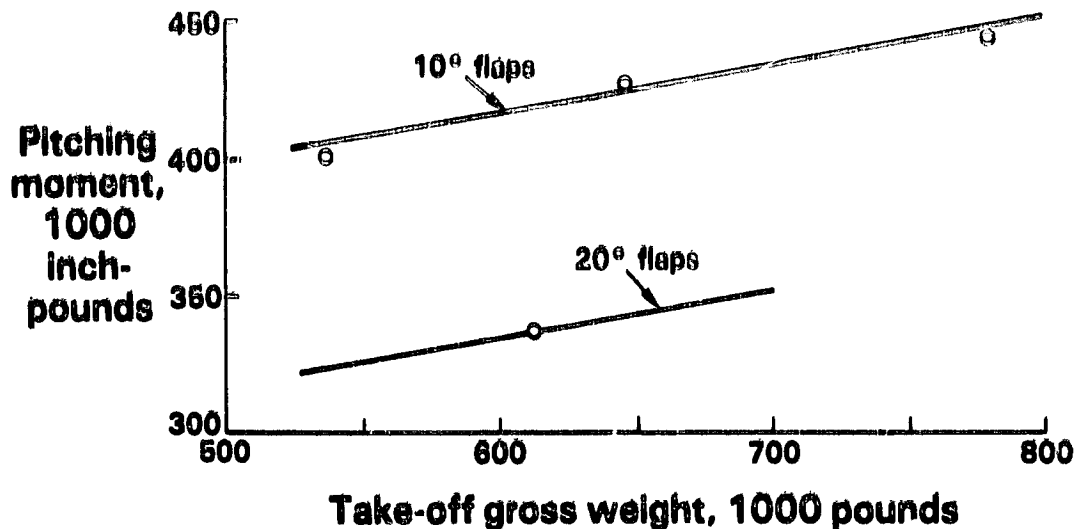
Figure 4-4   Pitching Moment at Take-Off versus Gross Weight and Flap
Setting.

The inertial loads for the 23 flight conditions are shown in Table 4-II
for the inboard engine and Table 4-III for the outboard engine. Normal
once-per-flight accelerations measured during take-off and typical
revenue flight did not exceed 1.3 G. The exceptions were the high G
turns (conditions 116, 117, 120, and 121) in which accelerations
reached 2 G's. In these cases, the differences between the G loads
measured at the airplane center of gravity and those measured at engine
numbers 3 and 4 were within the scatter of the data. This indicates
that the engine-mounted accelerometers sensed only the steady
accelerations of the whole airplane and that there were no significant
contributions from either wing or nacelle flexible (vibration-induced)
modes.

Similarly, the pitch rates during simulated normal revenue service did
not exceed 3 degrees/second with the peaks occurring prior to the
maximum aerodynamic load condition. The exceptions were the high G
turns and the airplane stall (condition 123) where the rates exceeded 6
and 5 degrees/second, respectively.
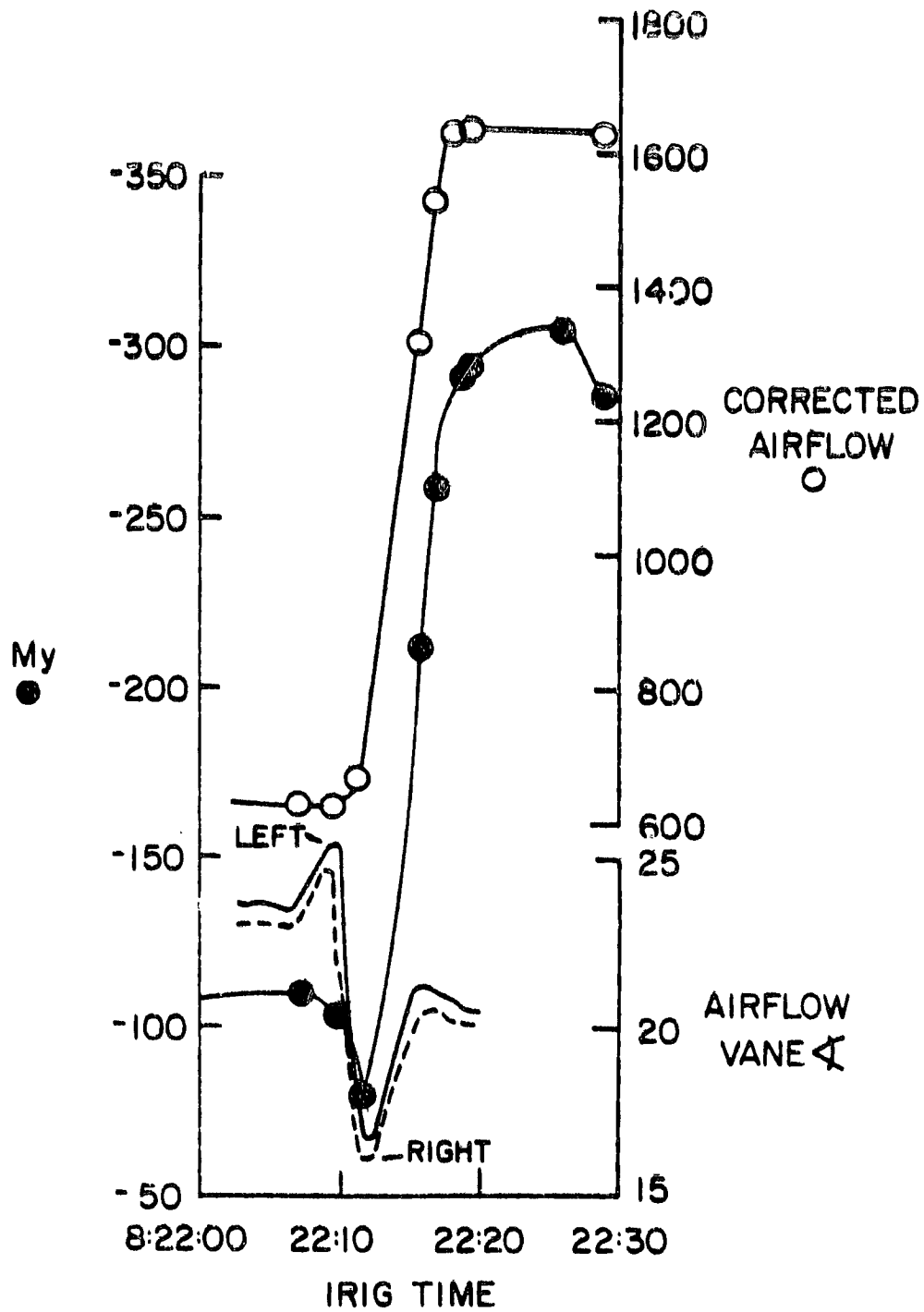
Figure 4-5 Pitching Moment Time History for the Stall Warning with 10-degree Flaps.

TABLE 4-II

INERTIAL DATA FOR ENGINE NUMBER 3

Cond	Lineal Acceleration G's			Angular Velocity Degrees/Second	
	A_z	A_y	A_x	Pitch	Yaw
101.1	-.30	-.15	1.08	.40	- .10
101.2	-.40	-.20	1.15	1.60	- .30
101.3	-.40	-.30	1.2	1.24	.65
118	-.35	-.10	1.2	1.98	.24
102	-.29	-.15	.955	- .60	- .70
103	NDA	-.1	.95	- .5	- .26
104	NDA	-.1	.98	- .25	- .13
105	NDA	-.1	.98	- .25	- .18
106	-.07	-.15	.99	- .53	- .20
107	NDA	-.1	1.04	- .24	- .18
108	-.09	-.20	.60	-1.9	.10
109	NDA	-.1	.91	- .20	- .37
110	NDA	-.1	1.24	.37	- .25
111	NDA	-.12	.91	- .74	- .49
112	NDA	-.1	1.04	0	- .18
113	NDA	-.1	.961	- .73	-1.64
114	NDA	-.1	1.1	.5	- .24
115	NDA	-.15	1.02	- .5	0
116	-.27	-.25	1.98	3.99	-1.8
117	-.25	-.40	1.60	6.49	-3.9
120	-.25	-.30	1.98	5.13	3.4
121	-.25	-.20	1.57	6.70	5.2
123	-.35	-.1	1.27	5.6	5.5

Acceleration coordinates are Nacelle axes per Figure 3-5.

Pitch rate: Positive, nose up.
Yaw rate: Positive, right turn.

NDA = Accelerometer Failed to Operate Properly.

TABLE 4-III

INERTIAL DATA FOR ENGINE NUMBER 4

Cond	Lineal Acceleration G's			Angular Velocity Degrees/Second	
	A_z	A_y	A_x	Pitch	Yaw
101.1	-.25	-.15	1.08	.40	.10
101.2	-.1	-.50	1.15	1.60	- .30
101.3	-.20	-.20	1.1	1.24	.65
118	-.25	-.20	1.1	1.98	.24
102	-.15	-.10	1.15	- .60	- .70
116	-.10	-.40	1.90	3.99	-1.8
117	-.15	-.30	1.50	6.49	-3.9
120	-.10	-.30	1.95	5.13	3.4
121	-.20	-.15	1.5	6.70	5.2
123	-.25	-.10	1.15	5.6	5.5

4.1.2 Transient Dynamic Loads

An analytical study of the "Effect of Time Dependent Loads on JT9D-7 Performance Deterioration", Reference 7, utilized Boeing-supplied data and the NASTRAN finite element mathematical model of the JT9D-7/747 propulsion system to evaluate the possible effect of a transient dynamic load on engine running clearance closures. Vertical wind gusts during flight, a typical landing, and a high sink rate, heavy gross weight landing were the conditions evaluated as possible candidates. The analysis showed insignificant additional clearance closure due to the vertical gust and normal landing cases but did indicate a possible dynamic load condition coincident with a hard landing. Therefore, it was planned during this flight test program to monitor any gust load.

The closest condition to a high sink rate (10 feet/second), normal gross weight (490,000-pound) landing that was achieved was a 5 feet/second, 690,000-pound landing. The vertical acceleration was 1.53 G's at the airplane CG (see Figure 3-6) and 1.7 G's and 2 G's at engine numbers 3 and 4, respectively. Normal landing accelerations were 1.1 G's at the airplane CG and 1.3g at the engines.

Gusts affect both aerodynamic and inertial loads, which must be considered simultaneously. The aerodynamic load arises directly from the change of inlet angle of attack associated with gust component of the relative wind. The inertial load is produced by the airplane's motion in response to the gust. No appreciable turbulence was encountered in the flight program, so this combined effect was not observed. Nevertheless, it was possible to establish the sensitivity of the inlet aerodynamic loads to angle of attack changes caused by gusts. In the simulated maximum dynamic pressure (q), push-over maneuver, loads were measured over a range of airplane angles of attack. From these data it was determined that the derivative of pitching moment with angle of attack at that Mach number and altitude was 87,736 inch-pounds per degree.

To put this figure in perspective, consider a maximum air speed condition, 375 knots Equivalent Air Speed (EAS) (747 maximum operating air speed) at an altitude of 20,000 feet. (This condition was chosen as a "worst plausible" case, much faster than economical climb, cruise, or holding speed.) At this altitude, a gust with a velocity of 36 feet/second can be expected about once in 800 hours of flying (Reference 10). The true air speed at this EAS and altitude is 984 feet/second, so that a gust with a velocity of 36 feet/second would produce an angle of attack change of 2.1 degrees. Allowing for the 8.5 percent higher actual (as opposed to simulated) dynamic pressure, a pitching moment change of 200,000 inch-pounds would be caused by the gust. This moment is about half of the nose-up pitching moment to be expected routinely at take-off.

4.1.3 Comparison With Past Predictions

The Pratt & Whitney Aircraft, "Effect of Steady Flight Loads on JT9D-7 Performance Deterioration" study, Reference 3, and "Performance Deterioration Based on Simulated Aerodynamic Loads Test," Reference 8, were both based on predicted inertial and aerodynamic loads provided by the Boeing Company. The measured and computed values based on the data from this program generally support the earlier predicted values with the following exceptions.

1. The actual aerodynamic shear loads and moments at the critical conditions (take-off and climb) were considerably higher than predicted. See Table 4-IV. This is partially due to higher actual angle of attack than predicted.

2. The cosine law for the circumferential pressure distribution assumed in the analysis of the simulated aerodynamic loads data is only a rough approximation of the actual distribution, especially in the critical region near the highlight.

3. The phase angle of the cosine distribution is about 20 degrees from the vertical near the highlight and approaches zero degrees farther into the inlet.

4. The accelerations were lower than predicted due mainly to the absence of vertical gusts included in the prediction but absent during flight testing (see Table 4-V).

4.1.4 Revision of Load Exceedence Curves

The flight test program was not long enough to generate sufficient statistical data to establish the basis for revisions to previously used exceedence curves. Exceedence curves are statistical plots which provide estimates of the number of times a load level is equaled or exceeded versus total number of flights. These curves are used to determine ratios of once-per-flight to once-per-several-flights loads.

The flight test, however, provided a basis for improved modeling of engine performance deterioration. Flight acceptance testing is performed over a narrow range of take-off gross weights, 500,000 to 550,000 pounds. Flap setting and pilot technique, however, will vary and, consequently, the loads experienced by different airplanes will vary. However, a 10-degree flap setting is typical of most production acceptance flights. Therefore, the 538,000-pound (condition 101-2) take-off was selected as representative of acceptance testing.

38

TABLE 4-IV

COMPARISON OF PREDICTED DATA WITH NAIL DATA
FOR "A"-FLANGE RESULTANT LOADS

CONDITION	PREDICTED VALUES				NAIL VALUES			
	F_x KIPS	F_y KIPS	M_x IN-KIPS	M_y IN-KIPS	F_x KI'	F_y KIPS	M_x IN-KIPS	M_y IN-KIPS
101 T.O. ROTATION [1]	3.9	-2.9	-162	-317	7.2	-2.9	-152	-401
102 EARLY CLIMB	3.5	-2.0	-90	-168	4.7	-1.1	-45	-206
103 MID CLIMB	2.3	-.9	-30	-52	4.1	-.6	-25	-126
104 HI MACH CR	1.8	-.8	-33	-57	2.5	-1.02	-36	-59
105 LO MACH CR	2.9	-1.4	-55	-95	3.5	-1.13	-42	-106
106 MAX MACH	1.6	-.5	-14	-16	.3	-.5	-16	19
107 IFSD	2.9	-1.2	-44	-79	3.3	-.7	-26	-85
108 MAX Q	-3.3	2.4	105	207	-1.4	1.9	29	-98
109 1.3 Vs, 0° FLAPS	6.2	-3.8	-185	-335	5.4	-1.4	-64	-243
110 1.3 Vs, 10° FLAPS	3.1	-2.1	-150	-294	6.2	-2.1	-97	-305
111 K1.3 Vs, 30° FLAPS	2.7	-1.5	-70	-130	3.9	-1.3	-73	-221
112 IDLE DESCENT	2.8	-1.5	-62	-109	4.1	-1.1	-30	-97
113 APPROACHE	3.6	-2.2	-93	-166	3.7	-1.4	-72	-202

[1] Previous values for 500K GWTO, 10° Flaps, 36000 lb thrust, Mach No. = 0.219
NAIL values for 500K GWTO, 10° Flaps, 32000 lb thrust, Mach No. = 0.25

TABLE 4-V

COMPARISON OF PREDICTED DATA WITH NAIL DATA FOR INERTIAL LOADS ON NUMBER 4 ENGINE

| | PREDICTED VALUES | | | | | NAIL RESULTS | | | | |
| | ACCEL g's | | | ANGULAR VEL DEG/SEC | | ACCEL G's | | | ANGULAR VEL DEG/SEC | |
CONDITION	n_x	n_y	n_z	$\dot{\theta}_x$	$\dot{\theta}_y$	n_x	n_y	n_z	$\dot{\theta}_x$	$\dot{\theta}_y$
101 △1	1.0	0	0	0	2.98	1.15	-.20	-.40	.30	-1.60
102	1.55	.13	0	.01	.92	.96	-.15	-.28	.70	.60
103	1.54	.17	0	.01	.57	.95	-.10	NDA	.26	.5
104	1.92	.19	0	.03	2.00	.98	-.10	NDA	.13	.25
105	1.92	.20	0	.02	1.32	.98	-.10	NDA	.18	.25
106	1.40	.12	0	0	.29	.99	-.15	-.07	.20	.53
107	1.32	.09	0	.01	.80	1.04	-.10	NDA	.18	.24
108	1.56	-.16	0	.01	.46	.60	-.20	-.09	.10	1.9
109	1.67	.12	0	.03	2.29	.91	-.10	NDA	.37	.2
110	1.70	.12	0	.03	2.35	1.24	-.10	NDA	.25	-.37
111	1.70	.12	0	.03	.80	.91	-.12	NDA	.49	.74
112	1.56	.12	0	.03	2.29	1.04	-.10	NDA	.18	0
113	1.70	.08	0	.04	3.09	.96	-.10	NDA	1.64	.73

NDA = No data acquired

△1 Previous values for 500K GWTO, 10° Flaps, 36000 lb thrust, Mach No. = 0.219
NAIL values for 500K GWTO, 10° Flaps, 32000 lb thrust, Mach No. = 0.25

Shortly after the airplanes enter revenue service, take-off gross weights will increase to the rated limits depending on routes being flown and the payload. Also runway lengths and ambient temperature variations will dictate flap settings and operating procedures. On this basis it was assumed that the heavy gross weight, 10-degree flap take-off conditions would be experienced within the first 50 flights by some airlines. This would increase the aerodynamic loads experienced by those airlines.

Finally, it was assumed that gust loads (based on earlier estimates), high G maneuvers, and airplane stall flight loads would occur randomly over the airplanes life during climb and cruise conditions. These flight loads and resultant clearance closures were then applied statistically to the climb and cruise to determine additional peak load and closure conditions occurring later in engine life. The rate of occurrence of each condition was based on Boeing- derived exceedence curves.

These assumptions were used in the final updating of the rub induced performance deterioration model.

4.2 CLEARANCE CLOSURES

The previously defined objectives of this program were to measure the flight loads on the nacelle/engine combination and the effects of these loads on the fan and high-pressure turbine clearance closures. However, it is the total closure in running clearances that causes the rubs and, hence, opening of running clearances and loss of performance. Therefore, the total axisymmetric and asymmetric closures in the fan and high-pressure turbine at the critical running clearances as well as the factors contributing to each type of closure in each module must be known. Only with this knowledge can methods be formulated to minimize clearance closure-induced rubs.

In the fan, there appear to be five types of loads that influence clearance closure, as shown in Figure 4-6A along with the causes of these loads. In the turbine there are six types of loads, as shown in Figure 4-6B along with their causes.

The laser proximity probes in the fans of the positions number 3 and 4 engines and in the first-stage high-pressure turbine of the position number 3 engine measured the absolute clearances, and recorded these measurements on video tape, 30 times per second. By comparing various combinations of these data from more than 100 engine hours of video tape data, it was possible to segregate the effects of rotor speed, altitude, thrust, aerodynamic and inertia loads, and thermal expansion.

SYMMETRIC CLOSURE

o ROTOR SPEED - POWER

o BLADE TIP AXIAL MOTION - POWER,
                          - ALTITUDE

FAN CLEARANCE
CLOSURE

NONSYMMETRIC CLOSURE

o BACKBONE BENDING - POWER

o AERODYNAMIC LOADS - ANGLE OF ATTACK,
                      - FAN AIRFLOW,
                      - DYNAMIC PRESSURE

o INERTIA LOADS - MANEUVERS
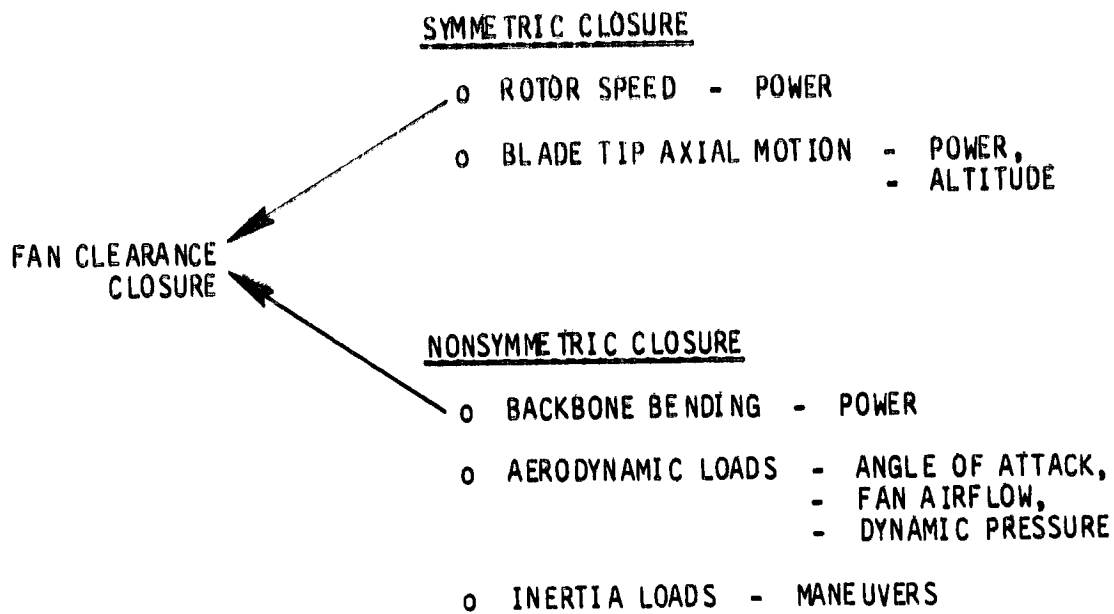
Figure 4-6A Fan Clearance Closure - Closure in the fan results from
engine power, altitude, angle of attack, fan airflow,
dynamic pressure, and maneuvers.

SYMMETRIC CLOSURE

o ROTOR SPEED - POWER

o THERMAL GROWTH OF
    DISK AND BLADES - TIME AT POWER

HIGH-PRESSURE TURBINE
CLEARANCE CLOSURE

NONSYMMETRIC CLOSURE

o BACKBONE BENDING - POWER

o AERODYNAMIC LOADS - ANGLE OF ATTACK
                      - FAN AIRFLOW
                      - DYNAMIC PRESSURE

o INERTIA LOADS - MANEUVERS

o THERMAL GROWTH OF
    CASE AND SE.LS - TIME AT POWER
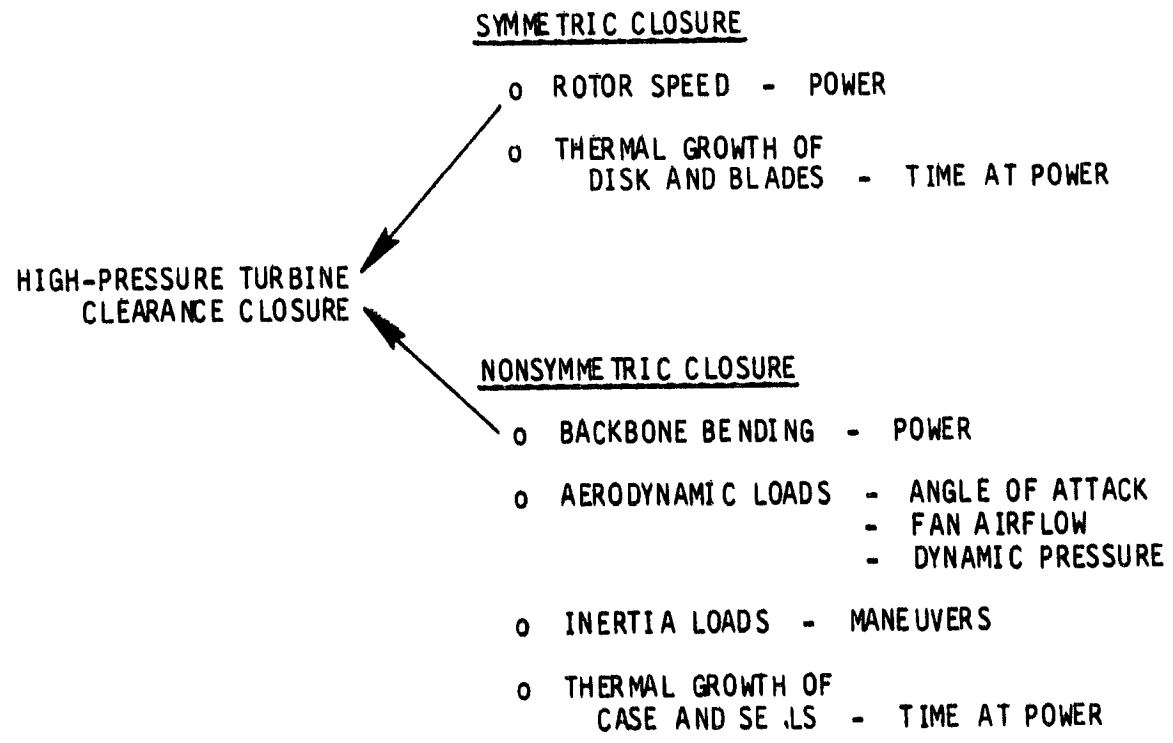
Figure 4-6B High-Pressure Turbine Clearance Closure - Closure in the
Turbine results from engine power, time at power, angle of
attack, fan airflow, dynamic pressure, and maneuvers.

4.2.1 Fan Clearance Closure

Running clearance closure between the fan blades and the outer air seal was at maximum during take-off, immediately following rotation. The pinch point was slightly inboard of bottom center of the engine. Tight clearances at the bottom also occurred during the airplane stall, stall warning, and high g turn maneuvers.

Analysis of the test data established that fan clearance closures are a combination of axisymmetric closures and asymmetric closures, as previously outlined on Figure 4-6A. Axisymmetric closures are caused by engine power-induced loads. The combination of centrifugal growth and axial deflection of the rotor/blade assembly establishes the axisymmetrical closures. Asymmetric closures are caused by both engine and externally generated forces. Backbone bending forces due to thrust deflect and ovalize the fan case, reducing running clearance at the bottom. Aerodynamic loads, further deflect the fan case. Finally, inertia loads cause additional asymmetric closures.

Axisymmetric closure is a maximum at altitude conditions when rotor speed is high and the gas path loading on the blades is low. Asymmetric closure is a maximum at take-off when the combined effect of thrust backbone bending and aerodynamic loads is greatest. The aerodynamic load is a function of the degree of turning of the fan inlet air stream (effective angle of attack) and the quantity of air turned (fan flow rate). Thus, the engine power level and take-off rotation angle establish fan clearance closure.

Measured fan clearance closures on the position numbers 3 and 4 engines were essentially equal as were flight loads under all flight conditions, indicating that fan rub-induced performance deterioration is independent of engine position.

Fan blade-to-case closure due to power effects is a combination of axisymmetric growth associated with low-pressure rotor (N_1) speed and asymmetric, thrust-induced, engine bending. Axisymmetric closure consists of fan blade and hub centrifugal and thermal growth, fan blade deflection due to gas-path loads, and case thermal growth.

The geometry of the fan outer air seal is such that forward axial bending of the fan blades, caused by gas-path loads, opens the blade tip clearance. However, at altitude lower gas-path loads, compared to sea level operation, are imposed on the fan blades, resulting in less bending of the blade and tighter axisymmetric running tip clearance.

Measured axisymmetric fan clearance change from a stabilized ground idle is presented in Figure 4-7 as a function of low-pressure rotor (N) speed, both on the ground and at altitude, based on ground and flight calibration data. The net thermal expansion effect on the fan rotor and case is also included in Figure 4-7. Axisymmetric clearance closures for the position number 3 fan at each of the test conditions are summarized on Table 4-VI, column 3.
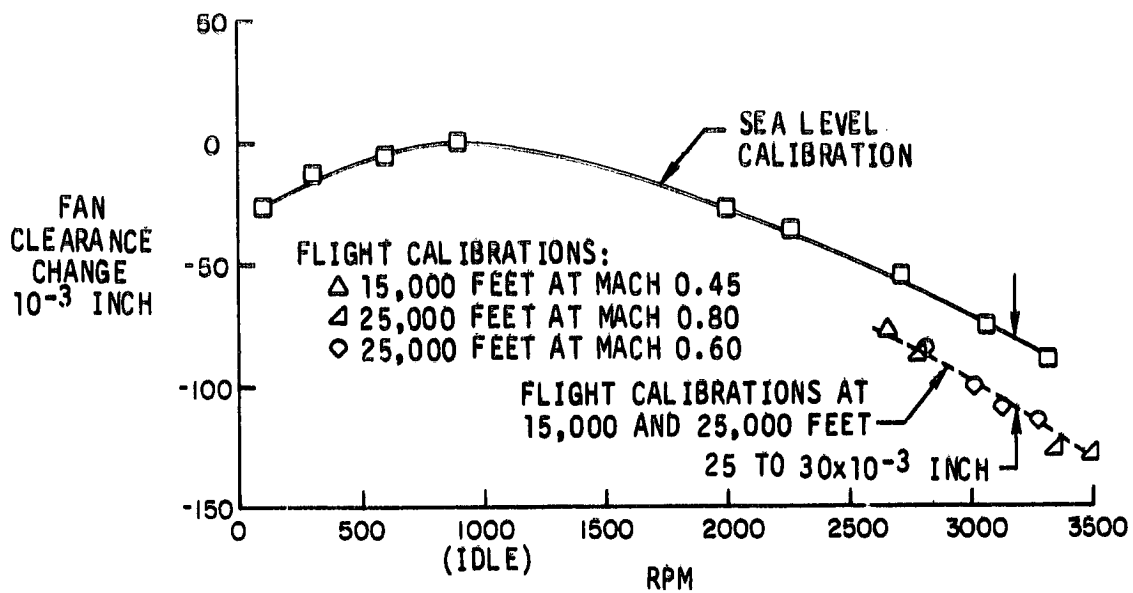
Figure 4-7 Measured Axisymmetric Clearance Change - Ground and flight calibration data show that clearances are tighter at altitude compared to sea level for a given engine speed.

Since the thrust reaction is carried through the thrust frame, which is offset 30 degrees above the engine horizontal centerline, there is a backbone bending moment generated about the engine horizontal axis. The resulting engine bending (as illustrated in Figure 4-8) causes the front flange of the fan case to deflect upward more than the front section of the low-pressure rotor which results in reduced fan blade clearance at the bottom of the engine. The thrust load effects on blade clearances in the position number 3 fan for each of the test conditions are shown on Table 4-VI, column 4.

Table 4-VI lists the fan maximum clearance closure and location of the pinch point for each of the test conditions as computed from the measured clearance values on position numbers 3 and 4 fans. The table also lists the axisymmetric closure and thrust-induced and flight loads-induced asymmetric closures for each condition. The axisymmetric closures are computed from the measured values and validated using the actual fan speed. The thrust and flight loads closures are computed using the NASTRAN finite element mathematical model of the JT9D/747 propulsion system using measured flight loads test data and computed thrust loads.

The thrust load effect on JT9D fan running clearances was computed using previously developed analytical models which were validated by test data from this program.

44
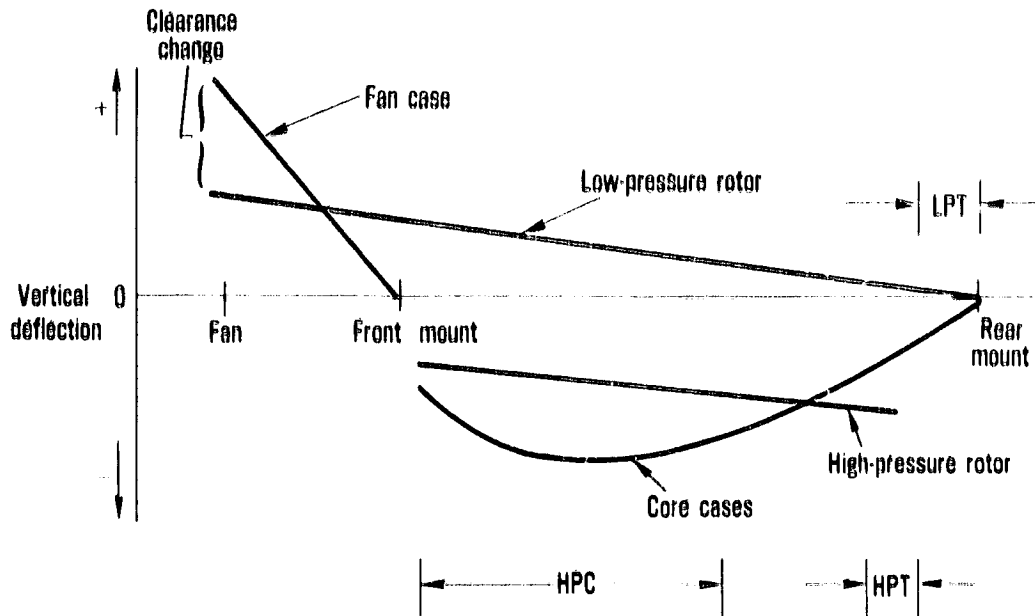
Figure 4-8   Typical Backbone Bending Plot for the JT9D Engine - A
backbone bending moment resulting from the engine thrust
reaction causes the front flange of the fan to deflect
upward more than the front section of the low-pressure
rotor.   (J24318-1)

The combined effects of power loads on fan running clearances are shown
on Figure 4-9 which plots the running clearance measured at the four
probe locations during a stabilized ground idle, run up to power,
ground calibration, and the first test take-off (101-1).   The probe
locations are shown in the lower left hand corner of the figure.
Engine power level is proportional to the plotted fan rotor speed
(N_1).   Reading from the left, the engine operated at stabilized
ground idle for 6 minutes.   The idle running clearance indicated at the
lower two probe locations is about 0.050 inch greater than at the upper
two probe locations due to the offset grind in the fan outer air seal.

The engine was then accelerated to approximately 80 percent of take-off
power.   As engine speed increased, the centrifugal force effect
axisymmetrically reduced the running clearance at all four probe
locations.   This effect can be seen in Figure 4-9 during the initial 10
seconds of the acceleration.   As the static thrust increase, the
resulting backbone bending effect opened the clearance at the top and
closed it further at the bottom of the engine.   The net effect at the
end of this acceleration was to close the clearances by 0.068 inch
axisymmetrically plus an additional 0.023 inch asymmetrically at the
lower probe locations.   At the subsequent increase to full power (640
seconds) there were additional closures with the axisymmetric and
asymmetric closures of about equal magnitude.

45

TABLE 4-VI

POSITION NUMBERS 3 AND 4 FAN CLEARANCE CLOSURES (INCH) RELATIVE TO GROUND IDLE

Flight Condition Description	Number	Mach number	Power Induced Closure Axisymmetric	Asymmetric (Thrust)	Position No. 3 Fan Flight Loads Closure	Total Closure	Other Closures	Measured Total Closure	Pinch Location*	Position Number 4 Fan Measured Total Closure	Pinch Location*
612,000 lb Take-Off with 20 Flaps	101-1	0.25	-0.086	-0.032	-0.125	-0.243	+0.022	-0.221	203	-0.223	193
533,000 lb Take-Off with 10 Flaps	101-2	0.24	-0.087	-0.037	-0.139	-0.263	+0.025	-0.238	197	-0.251	195
647,000 lb Take-Off with 10 Flaps	101-3	0.25	-0.087	-0.037	-0.147	-0.271	+0.016	-0.255	--	-0.263	195
780,000 lb Take-Off with 10 Flaps (Simulated)	118	0.30	-0.088	-0.041	-0.149	-0.278	+0.008	-0.270	--	-0.285	194
Low-Climb	102	0.37	-0.082	-0.036	-0.074	-0.192	-0.025	-0.217	206	-0.208	198
Mid-Climb	103	0.60	-0.085	-0.025	-0.056	-0.166	-0.026	-0.192	207	-0.181	196
High Mach Number Cruise	104	0.86	-0.107	-0.016	-0.033	-0.156	+0.008	-0.148	220	-0.145	198
Low Mach Number Cruise	105	0.77	-0.099	-0.011	-0.049	-0.159	+0.007	-0.152	216	-0.153	198
Maximum Mach Number Flight	106	0.91	--	--	--	--	--	-0.150	219	-0.140	194
In-Flight Relight	107	0.72	-0.059	-0.008	-0.045	-0.112	--	**	--	Not Shut Down	
Maximum Dynamic Pressure Flight	108	0.84	-0.124	-0.034	-0.023	-0.135	-0.027	-0.162	220	-0.125	212
Stall Warning with Flaps Up	109	0.37	-0.094	-0.025	-0.086	-0.205	--	**	--	-0.124	203
Stall Warning with 10 Flaps	110	0.35	-0.090	-0.027	-0.108	-0.225	--	-0.171	204	-0.199	199
Stall Warning with 30 Flaps	111	0.27	-0.113	-0.028	-0.075	-0.216	+0.018	-0.198	205	-0.113	212
Idle Descent	112	0.44	0.0	-0.001	-0.054	-0.055	-0.012	-0.067	199	-0.063	206
Approach	113	0.27	-0.117	-0.038	-0.069	-0.224	+0.028	-0.196	204	-0.182	202
Touch and Go	114	0.26	0.087	-0.047	-0.085	-0.219	+0.030	-0.189	210	-0.145	206
Thrust Reverse	115	0.18	-0.070	-0.036	-0.009	-0.043	-0.025	-0.058	240	-0.058	208
2.0-G Left Turn with Flaps Up	116	0.49	-0.095	-0.017	-0.100	-0.212	+0.011	-0.201	208	-0.139	194
1.6-G Left Turn with 30 Flaps	117	0.26	-0.057	-0.036	-0.137	-0.230	--	**	--	-0.103	199
2.0-G Right Turn with Flaps Up	120	0.48	-0.068	-0.016	-0.081	-0.165	+0.018	-0.147	195	-0.158	188
1.6-G Right Turn with 30 Flaps	121	0.27	-0.100	-0.028	-0.080	-0.208	-0.099	-0.217	193	-0.173	205
Airplane Stall	123	0.21	-0.116	-0.036	-0.094	-0.246	-0.014	-0.260	190	--	--

* Measured clockwise from top of engine, as viewed from the rear.
** Insufficient laser proximity probe data to define pinch point.

Note: Negative values of closure may be interpreted as reduced clearance and increased chance of rubs.
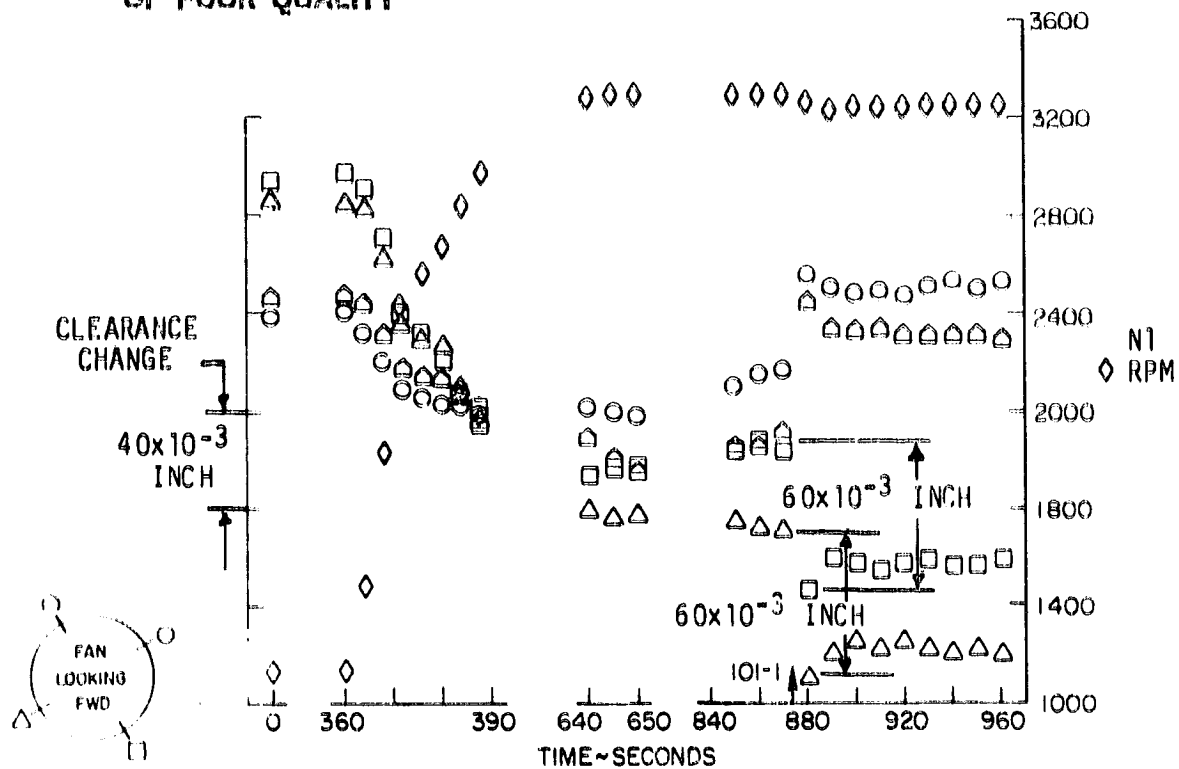
Figure 4-9   Change in Fan Running Clearance from Stabilized Ground Idle
            to the First Take-Off - Take-off at 612,000 pounds with
            20-degree flaps resulted in a 0.060-inch closure in the
            position number 3 fan.

The significant flight loads, which occurred during conditions of high
power and high angle of attack (Table 4-I), were in an upward and
slightly outboard direction due to the effect of the fuselage on inlet
airflow.   These loads on the inlet were transmitted to the fan cases
causing an additional upward and slightly outboard deflection.   This
effect is seen in Figure 4-9 immediately following take-off rotation
(condition 101-1) when this force is a maximum.   The measured
clearances open at the top and close at the bottom.

The computed flight load induced closures at the pinch positions for
this take-off and the test conditions are listed in column 5 on Table
4-VI based on NASTRAN model and the measured flight loads.

Column 6 on Table 4-VI sums the three computed closure effects for each
test condition at the pinch location.   The difference (column 7)
between this value and the estimated pinch position closure based on
laser measured closures (column 8) represents the sum of possible
measurement errors and NASTRAN model limitations.

The effects of take-off flap angle and gross weight on flight loads
(Figure 4-4) also apply directly to fan clearance closures and rub as
shown on Figure 4-10.

47
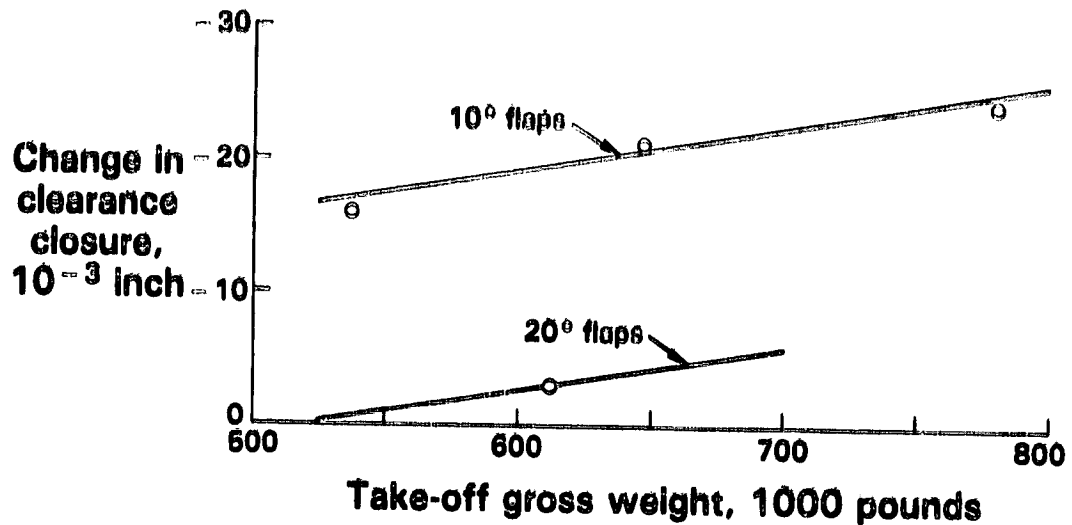
Figure 4-10 Effect of Take-Off Gross Weight and Flap Setting on Local
Fan Clearance Closure at Take-Off - Change in flap setting
has greater effect than gross weight on fan clearance
closure and rub depth.

The stall warning (conditions 109, 110, and 111), the inadvertant stall
(condition 123), and the high G turns (conditions 116, 117, 120, and
121) also presented conditions of combined high power and angle of
attack with resultant high aerodynamic loads and significant fan
clearance closures.

Fan running tip clearance changes were measured on both the inboard and
outboard engines of the test 747. The laser proximity probes were
placed at the same circumferential locations in each fan case to
ascertain the effect of engine position on both the magnitude and
direction of fan closure. As illustrated on Table 4-VI, there is
slight difference in the maximum pinch clearance closure on the inboard
and outboard engines.

4.2.2 High-Pressure Turbine Clearance Closure

As in the fan, blade-seal rubs in the turbine occur when the combined
effect of engine power-induced and flight load-induced clearance
closures exceed the build clearances. As seen in Figure 4-6B, there is
an additional effect, namely differential thermal expansion, which
contributes to both symmetric and nonsymmetric clearance closure in the
turbine.

During the conditions of maximum thrust and aerodynamic loads, that is,
high power and high angle of attack, these effects are additive and
both will deflect the turbine case upward against the rotor.

48

Maximum closure was measured in the lower right hand quadrant of the first-stage high-pressure turbine under two conditions. The first condition is after extended (over 10 minutes) high power operation on the ground when the thrust, centrifugal, and differential thermal expansion effects are all maximum. The second is a flight condition which combines high power and high aerodynamic loading.

The power- and aerodynamic load-induced closure effects for the planned test conditions plus an additional climb condition and ground calibration are listed on Table 4-VII. Note that the axisymmetric closure for the first condition was not typical since the take-off closure for the first condition was not typical since the take-off followed a ground calibration where differential thermal expansion was significant. In the typical revenue flight, maximum closure occurred during climb at 20,000 feet (pinch point on Table 4-VI) and also following a snap to reverse thrust after landing. The ground calibration and stall warning were other acceptance test conditions that induced high power aerodynamic load-induced closures.

The various effects contributing to high-pressure turbine clearance closure in a typical take-off and climb are shown in Figure 4-11. The upper plot of this figure shows the high-pressure rotor speed and clearance change at the four laser probes versus time. The overlay on the lower plot shows the axisymmetric closures as the upper solid line. The initial closure is due to the centrifugal effect with engine acceleration. The subsequent changes then occur due to the combined effect of disk and blade thermal expansion and case uniform thermal expansion. The case expansion opens the clearance and is dominant for the initial 40 seconds. The combined effect of blade and disk expansion, which is slower, then becomes dominant and continues to uniformly close down clearances out into the climb. The thrust backbone bending-induced closure at the bottom of the engine is shown on the lower plot of the figure as the upper cross hatch. This closure increases initially, drops slightly as the airplane goes down the runway, then decreases further during climb. The aerodynamic load-induced closure, shown in the lower cross hatch, is a maximum immediately after take-off rotation when inlet angle of attack is a maximum. It then decreases during climb as this angle decreases. The thrust load and aerodynamic load effects were computed using the NASTRAN analytical model and validated using measurements from this test where thrust- and aerodynamic-load effects could be isolated.

The differences between the sum of the axisymmetric, thrust, and aerodynamic load-induced closures and the measured closures are identified as the asymmetric thermal load effect (Column 5 on Table 4-VII). This effect builds with time at high power as shown by the spread between the two lower probe closure measurements on Figure 4-11.

The clearance closure at thrust reverse (condition 115) is a power effect. The deceleration during approach initiates an engine cool-down with the case cooling faster than the disk. When the engine is accelerated in the reverse thrust mode, the centrifugal effect expands

TABLE 4-VII

POSITION NUMBER 3 HIGH-PRESSURE TURBINE CLEARANCE CLOSURES (INCH) RELATIVE TO GROUND IDLE AT 180-DEGREE CIRCUMFERENTIAL LOCATION

Flight Condition Description	Number	Estimated Thrust (pounds)	Power Induced Closure				Flight Loads Closure	Measured Total Closure
			Axisymmetric (Speed + Thermal)	Asymmetric (Thrust Load)	Asymmetric (Thermal Load)	Estimated Total		
612,000 lb Take-Off with 20 Flaps	101-1	32,000	-0.036	-0.010	+0.002	-0.044	-0.007	-0.051
538,000 lb Take-Off with 10 Flaps	101-2	31,000	-0.004	-0.009	+0.002	-0.011	-0.008	-0.019
647,000 lb Take-Off with 10 Flaps	101-3	30,000	-0.005	-0.009	0.000	-0.014	-0.009	-0.025
780,000 lb Take-Off with 10 Flaps (Simulated)	118	31,000	-0.016	-0.009	+0.002	-0.023	-0.009	-0.032
Low-Climb	102	25,000	-0.026	-0.007	-0.004	-0.037	-0.004	-0.041
Pinch Point		20,000	-0.031	-0.006	-0.005	-0.042	-0.004	-0.045
Mid-Climb	103	18,000	-0.031	-0.005	-0.001	-0.037	-0.003	-0.040
High Mach Number Cruise	104	9,000	-0.030	-0.003	-0.001	-0.034	-0.001	-0.035
Low Mach Number Cruise	105	8,000	-0.024	-0.002	-0.004	-0.030	-0.002	-0.032
Maximum Mach Number Flight	106	9,000	-0.026	-0.003	-0.003	-0.032	0.000	-0.032
In-Flight Relight	107	5,000	-0.039	-0.002	+0.001	-0.040	-0.002	-0.042
Maximum Dynamic Pressure Flight	108	14,000	-0.036	-0.004	-0.003	-0.043	+0.002	-0.041
Stall Warning with Flaps Up	109	17,000	-0.028	-0.005	+0.004	-0.029	-0.005	-0.034
Stall Warning with 10 Flaps	110	20,000	-0.029	-0.006	+0.003	-0.032	-0.006	-0.038
Stall Warning with 30 Flaps	111	20,000	-0.037	-0.006	0.000	-0.043	-0.004	-0.047
Idle Descent	112	0	0.000	0.000	+0.004	+0.004	-0.002	+0.002
Approach	113	27,000	-0.022	-0.008	-0.001	-0.031	-0.004	-0.035
Touch and Go	114	34,000	-0.025	-0.010	+0.002	-0.033	-0.005	-0.038
Thrust Reverse	115	26,000	-0.034	-0.008	-0.001	-0.043	0.000	-0.043
2.0-G Left Turn with Flaps Up	116	22,000	-0.033	-0.007	-0.001	-0.041	-0.005	-0.045
1.6-G Left Turn with 30 Flaps	117	25,000	-0.031	-0.008	+0.002	-0.037	-0.006	-0.043
2.0-G Right Turn with Flaps Up	120	8,000	-0.019	-0.003	-0.002	-0.024	-0.005	-0.029
1.6-G Right Turn with 30 Flaps	121	21,000	-0.025	-0.006	+0.001	-0.030	-0.005	-0.036
Airplane Stall	123	26,000	-0.031	-0.008	+0.002	-0.037	-0.007	-0.044
Hard Landing		20,000	-0.024	-0.006	-0.004	-0.034	0.010	-0.020
Ground Calibration		48,000	-0.036	-0.014	+0.002	-0.048	0.009	-0.048

Note: Negative values of closure may be interpreted as reduced clearance and increased chance of rubs.
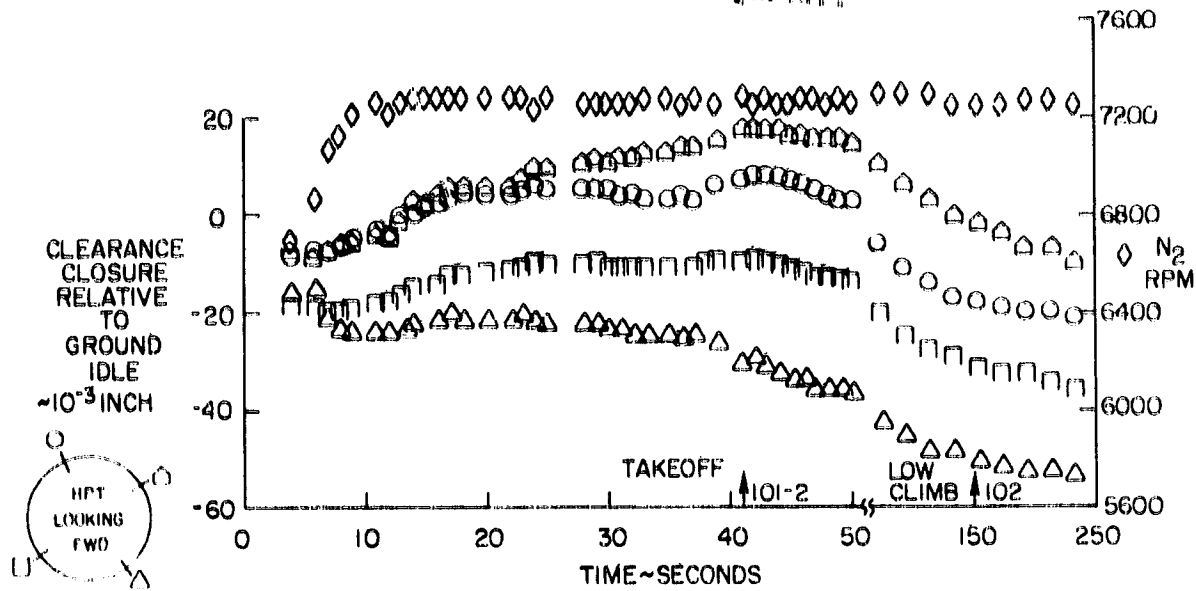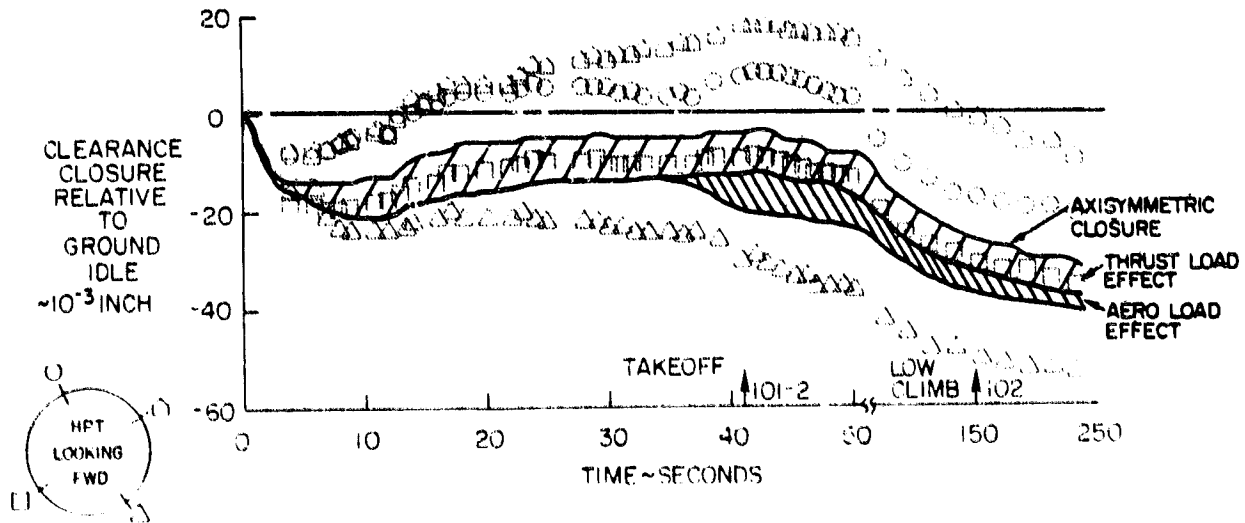
Figure 4-11 Axisymmetric and Asymmetric Clearance Closures During Typical Take-Off and Climb - The minimum clearance pinch occurred about 200 seconds into the climb.

51

the rotor faster than the cool turbine case can expand. This deceleration/acceleration effect is explained in detail in the "In-Service Engine Data Report", Reference 5.

The clearance closures during the stall warning, (condition 111), avoidance maneuver (condition 116), and airplane stall (condition 123) each combine high power and high angle of attack maneuvers. Thus the centrifugal, thermal, thrust bending, and aerodynamic effects are all large and contribute to clearance closure at the bottom of the engine.

The approach (condition 113) and touch and go (condition 114) test flights show aerodynamic flight load effects also. These effects also are due to the combined effect of high angle of attack and power level. Note that for the touch and go the high data point was recorded following the rotation and, hence, was similar to take-off.

Data for the remaining test conditions were taken during level flight, and the flight load effects were insignificant.

4.3 DYNAMIC LOADS EVALUATION

During flight, the engine is subjected to three types of loads. Normal flight at constant thrust, altitude, and heading subjects the engine to steady state loads. During a thrust change or controlled maneuver, quasi-steady state loads are imposed on the engine. Dynamic loads on the engine result during a sudden inertia load such as that caused by a significant vertical gust or a hard landing. The effects of such dynamic loading on the JT9D engine were investigated during an analytical study conducted as part of the third phase of the Engine Diagnostics Program. The results of this study, presented in Reference 7, included a prediction that an insignificant level of JT9D-7 engine performance deterioration would occur as a result of a vertical gust encounter. The hard landing case was more complex, and a firm quantitative estimate of the extent of rub damage could not be analytically determined. Therefore, the hard landing case was added to this Flight Loads Test program to experimentally measure the effect of a hard landing on fan and high-pressure turbine running clearances and engine performance.

No Gust loads were experienced during the flight test program. However, as discussed in Section 4.1.2, the worst plausible gust would have caused an equivalent aerodynamic load less than one-half that experienced at take-off such that the resulting closures would not have been significant.

The hard landing was conducted at the end of the fourth test flight at an estimated sink rate of 5 feet/second and an airplane gross weight of 690,000 pounds. Both approach power level and airplane angle of attack were greater than normal due to the high gross weight. Hence, the resulting aerodynamic plus thrust load-induced fan clearance closure was much greater than normal for the landing approach.

52

At touch down the fan clearance as measured by the laser probes closed an additional 0.015 inch, then opened when the engines were throttled back prior to thrust reversal (see Figure 4-12). The tightest fan clearance was equal to that at maximum gross weight take-off. There were no sharp surges in laser monitored fan blade tip clearance at the time of touch down. Neither were there any marks in the fan rub strip to indicate sudden impact with the fan blades.
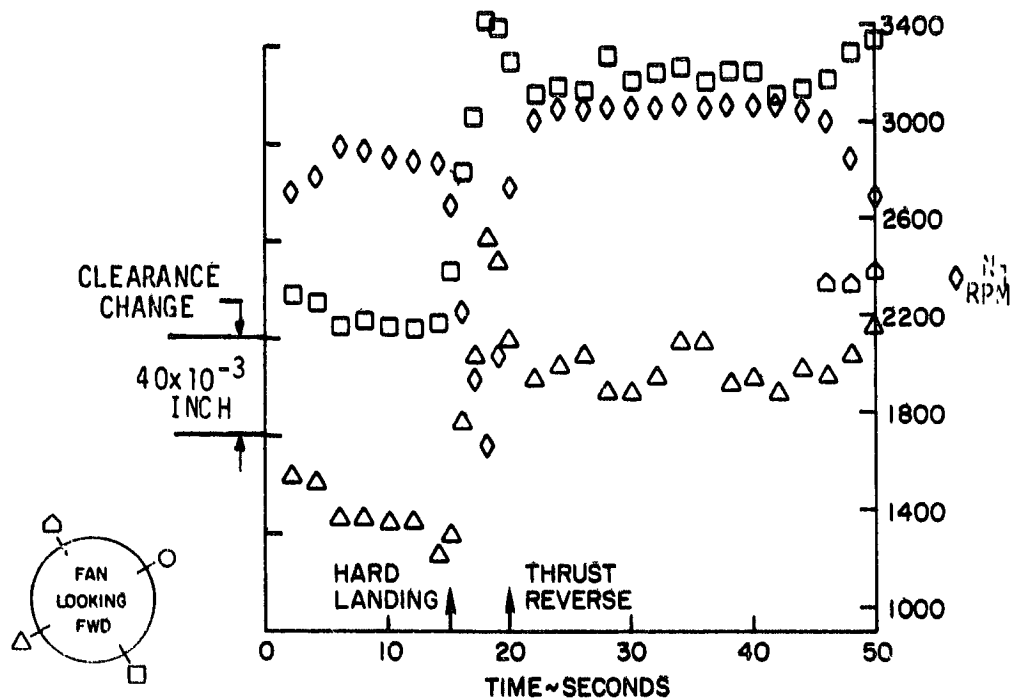
Figure 4-12 Effect of a Hard Landing on Fan Clearance - The landing at a 5 feet/second sink rate and 690,000-pound gross weight had only a small effect on clearance in the fan of the position number 3 engine.

High-pressure turbine laser measured running clearance, as shown in Figure 4-13, also indicated no sudden clearance closure at touch down. The net effect was that the impact of the high sink rate landing had small effect on fan clearance and no effect on turbine clearance. The combined effect of aerodynamic forces and impact force would be even less in a high sink rate landing of a revenue service airplane where landing gross weights would not exceed 600,000 pounds.

In summary, the dynamic load test results were not as conclusive as could be desired, but the indications were that dynamic loads are not the cause of rub-induced blade seal wear.

53
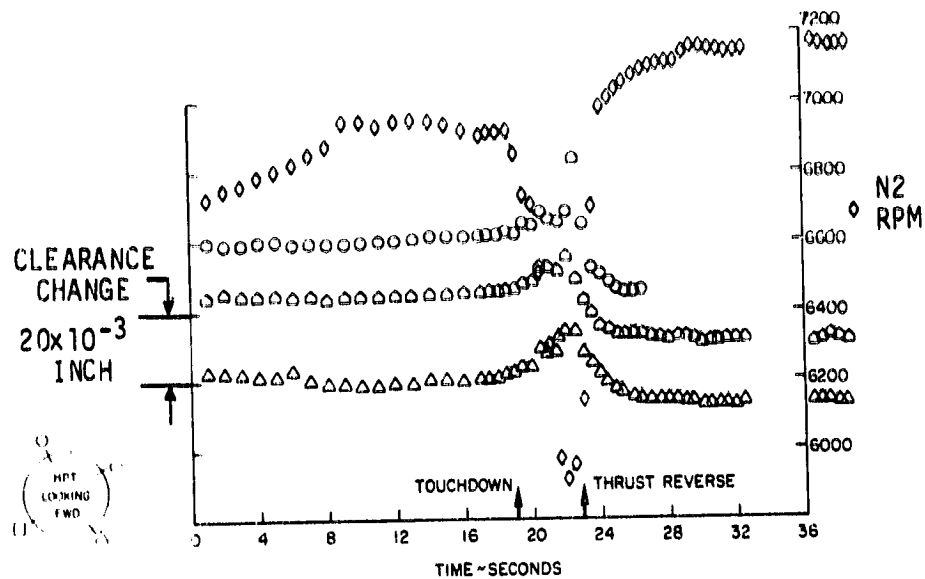
Figure 4-13 Effect of a Hard Landing on High-Pressure Turbine
Clearance - The landing at a 5 feet/second sink rate and
690,000-pound gross weight had no effect on clearance in
the high-pressure turbine of the position number 3 engine;
clearance closure occurred later when engine was
accelerated in thrust reverse mode.

4.4 MEASURED PERFORMANCE CHANGES

Preflight and postflight engine calibrations measured the rub-induced
performance deterioration. The results validated prior predictions
(Table 4-VIII). Fan performance decreased progressively through the
program due to increasing aerodynamic loads. High-pressure turbine
performance deterioration occurred during initial preflight
calibrations when extended high power operations maximized the
clearance closure due to centrifugal, thrust bending, and thermal
growth effects. This closure caused the turbine rub. Clearance
measurements during these ground tests and subsequent flight tests
indicated that had rub not occurred earlier, it would have occurred
during climb.

The test engine installed in number 3 position (S/N 662204) was a high
time JT9D-7A engine which was partially rebuilt for the test program.
A new fan outer air seal was installed to overhaul standards in
combination with high time fan blades to achieve near-production fan
build clearances.

54

The high-pressure turbine was rebuilt with new first- and second-stage blades, new second-stage vanes, and new outer and inner gas-path seals. The second-stage blade clearances were within engine build specification values. However, the first-stage blade clearances were built about 0.006 inch tighter than new engine build clearances. Thus, the test program was expected to result in rub and deterioration of the fan performance equal to the level of that in a new fan undergoing the planned test conditions. The high-pressure turbine performance deterioration was expected to be slightly greater due to the initial tight clearance of the first stage. Finally, no deterioration was expected in the remaining engine modules. The results of the program showed the expected rub-induced performance loss as compared with prior data (Table 4-VIII). Performance change resulting from this program is discussed in detail in Reference 2.

TABLE 4-VIII

COMPARISON OF NAIL PROGRAM MODULE DETERIORATION
WITH PREVIOUS PROGRAM RESULTS

Module	Historical Data Analysis (149 Cycles)	In-Service Engine Analysis (150 Cycles)	P&WA Testing of P-695743 (141 Cycles)	Simulated Aero Loads Test	NAIL Flight Test of P-662204
	Change in TSFC (%) at Sea Level Static Take-off Thrust				
Fan	+0.1	+0.2	+0.1	+0.2	+0.2
Low-Pressure Compressor	+0.2	+0.4	+0.4	+0.3	-
High-Pressure Compressor	+0.3	+0.2	+0.3	+0.2	-
High-Pressure Turbine	+0.4	+0.4	+0.6	+0.5	+0.5
Low-Pressure Turbine	+0.5	+0.1	+0.1	+0.1	-
Total	+1.5	+1.3	+1.5	+1.3	+0.7

4.5 MODEL REFINEMENTS

A JT9D engine performance deterioration prediction model has been developed in the Engine Diagnostics Program. This model predicts the JT9D-7 engine deterioration with usage due to the effects of the three principle causes: blade-to-seal rubs, erosion in the cold section, and airfoil thermal distortion in the hot section.

This final phase of the Engine Diagnostics Program developed a better understanding of the causes and effects of blade-to-seal rubs and the resulting opening of running clearances throughout the engine. As previously stated, clearance closures, which result in rubs when the build clearances are exceeded, are caused by a combination of flight- and power-induced loads. This final phase evaluated those clearance closures and rubs caused by airplane acceptance testing and simulated revenue service and made a final refinement of the model based on these results.

The model uses a NASTRAN finite element model of the JT9D-7 for calculation of aerodynamic load, inertia load, gyroscopic load, and thrust bending load-induced asymmetric clearance closures. These closures, the initial build clearances, the axisymmetric closures, and any thermally induced asymmetric closures are combined with abradability factors in a postprocessor to determine blade and seal rubs in each stage at each flight condition and power setting. Performance influence coefficients are applied to the clearance changes in each stage to determine the performance change in each engine module. The final model of performance deterioration with engine usage was then determined by selecting the likely extreme operating conditions to which the airplane engine will be subjected, computing the performance deterioration with each condition, and plotting this likely deterioration with usage. Figure 4-14 is such a plot for the JT9D-7. Note that usage is plotted as flight cycles rather than hours since the three primary performance deterioration modes are functions of take-off cycles more than of flight hours.

The engine and module performance deterioration models were developed based on the initial historical data (Reference 4). Then they were updated and refined based on the results of each successive phase of the Engine Diagnostics Program. These models, which are shown in Section 6 of Reference 2, relate the engine performance loss from new (changes in thrust specific fuel consumption and exhaust gas temperature) and the module performance loss (changes in efficiency and flow capacity) to engine flight cycles from the initial acceptance flight through 2000 revenue flight cycles. The models assume no engine repair out through 2000 cycles. The exception is the high-pressure turbine where hot section maintenance is assumed to start after 1000 flight cycles. Subsequent repair of hot and cold sections is assumed to maintain performance at or near the 2000 cycle level.

56
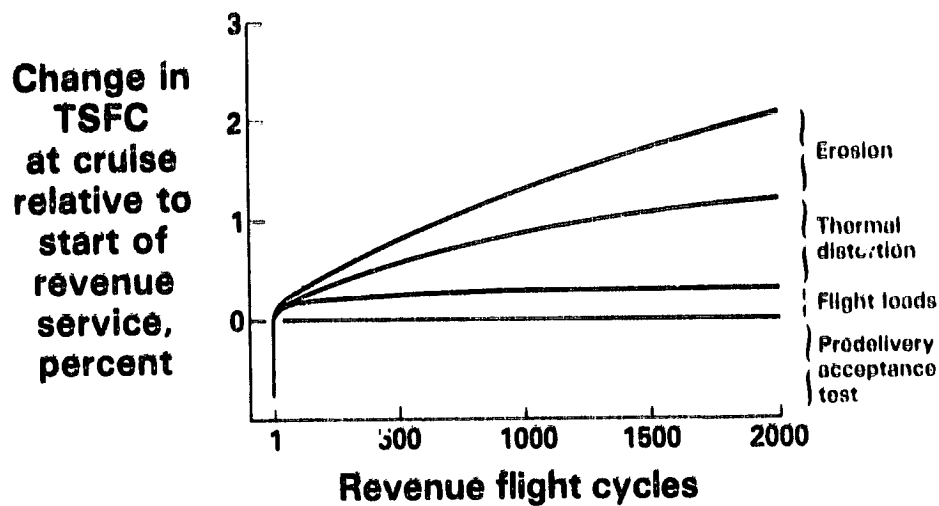
Figure 4-14   JT9D-7 Engine Performance Deterioration at Cruise.
(J26216-21)

All known contributors to the performance loss are included in the deterioration models. These damage mechanisms include blade-to-seal clearance increases in all stages resulting from rubs due to flight loads, thrust bending of cases, and centrifugal and thermal expansion effects; changes in cold section airfoil geometry, blade-to-seal clearances and surface roughness due to erosion of blades and seals; and finally thermal distortion of hot sections parts due to extended high temperature operation and changes in temperature pattern factors.

This final revision of the JT9D-7 Performance Deterioration Model incorporates the following changes relative to the models developed from the earlier phases of the Engine Diagnostics Program (Reference 8).

1. Input aerodynamic, inertia, and gyroscopic load effects were based on loads computed from the actual measured inlet pressures and accelerations from the Flight Loads Test program. The critical aerodynamic loads on the inlet (at take-off) were 36 to 80 percent greater than the estimated loads used previously.

2. Axisymmetric closure in the high-pressure turbine was revised to reflect the measured case thermal response which was more rapid than previously estimated.

3. The combination of flight conditions which represents a typical production acceptance flight (first flight prior to airplane delivery) was established by Boeing as a 550,000 pounds gross weight, full power, take-off with 10-degree flaps. Clearance closures measured in conditions 101-2 and 102 through 115 were used to establish the acceptance flight performance bases.

4. Additional rub-induced performance deterioration during early revenue service assumed that the rubs resulting from heavy gross weight (780,000 pounds), full power take-off with 10-degree flaps (condition 118) are likely to be encountered in the initial 50 revenue flights.

5. Longer term rub-induced deterioration is assumed to be caused by random instances of gust (based on prior estimates), high G turns (conditions 116, 117, 120 and 121), and stall-induced (condition 123) clearance closures occurring as additional closures during the climb and cruise conditions in revenue flight. The probability of occurrence of these additive effects during climb and cruise are based on the Boeing exceedance curves plotted on Figures 40, 41 and 42 in Reference 3.

6. Tip clearance influence coefficients on engine performance were updated to reflect results of the latest in-house testing and analysis of the JT9D components.

A complete discussion of how the measured and calculated running clearance changes, measured rubs, and measured performance changes were used to update the performance deterioration prediction models is included in Section 6 of Reference 2.

The breakdown of engine deterioration with usage by module and by primary deterioration mode as determined by the final refined model is summarized on Figure 4-15. It shows the change in thrust specific fuel consumption at take-off condition following the acceptance flight prior to delivery, then after the 500th, 1000th, and 2000th revenue flights. Note that the model assumes hot section repair after 1000 flights to stabilize high-pressure turbine deterioration. Note that the low-pressure compressor and high-pressure turbine are the prime contributors to rub-induced performance loss.

The comparable increase in engine exhaust gas temperature (EGT) at take-off engine pressure ratio (EPR) level is:

	Completed Flights			
	1	500	1000	2000
Exhaust Gas Temperature Increase (°C)	11	18	24	30

58
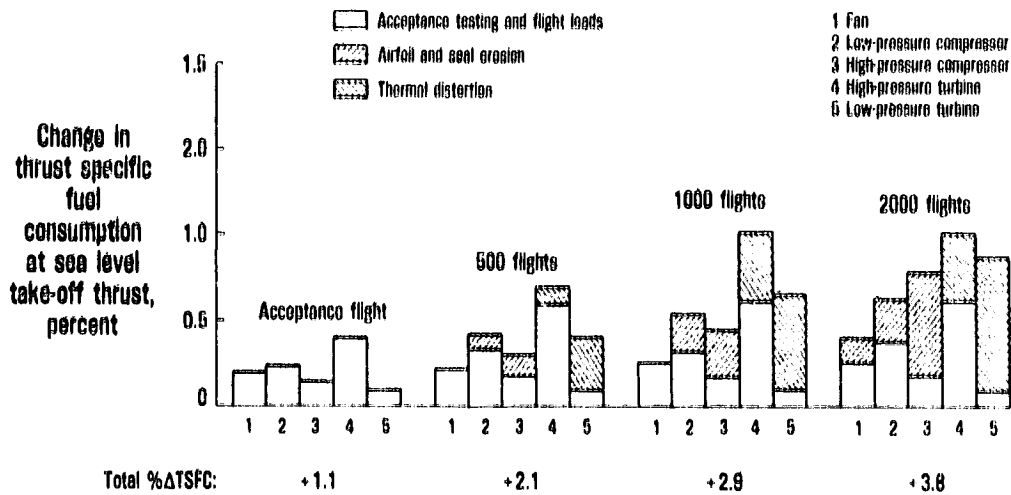
Figure 4-15   Module Performance Deterioration Relative to Production
              as Predicted by the Final Model.   (J26090-15)

The relation between performance loss at take-off (ground) conditions
and performance loss at cruise (altitude) conditions was originally
established in the in-service data evaluation phase (Reference 5) and
confirmed with the flight test data.

It should be noted that in-flight data cannot directly define actual
thrust specific fuel consumption loss because of the lack of thrust
measurement. Also, the limited number of measured parameters provide
less insight into individual module contributions to performance
losses. To accurately model in-flight thrust specific fuel consumption
deterioration, it is necessary to start with sea level test stand data
where both thrust and fuel flow, as well as sufficient parameters to
make reasonable assessments of individual component contributions, are
measured. Detailed part assessment and loads testing or structural
simulation are necessary to further establish causes (clearance,
erosion, etc.) by component. The model can then be confirmed at sea
level against a variety of test data. The model then has sufficient
validity to be exercised at cruise conditions and compared with cruise
data. This is the approach established in the JT9D Engine Diagnostics
Program.

Engine flight performance deterioration was determined to be less at
cruise than on the ground because the sensitivity to module
deterioration is reduced by the ram effect which increases the

59

effective engine pressure ratio at cruise. This relationship is based on flight data and Pratt & Whitney Aircraft altitude test facility data. Cruise performance thrust specific fuel consumption change is about 75 percent of ground thrust specific fuel consumption change with usage.

The combined effect of the model refinements and ground-to-flight deterioration rate correction are shown on Figure 4-14. This figure identifies the rub-induced performance loss which occurs in acceptance testing. It also identifies the deterioration caused by rub, erosion, and thermal distortion that is predicted to occur in typical revenue service which includes maximum gross weight operation. An increase of 2.1 percent in cruise thrust specific fuel consumption from all causes is predicted for 2000 revenue flight cycles.

60

SECTION 5.0

CONCLUSIONS

5.1 OVERVIEW

The Pratt & Whitney Aircraft JT9D Flight Loads Test/Boeing-NAIL Program was a highly successful joint program, both in its execution and in the results achieved. Sponsorship by two different National Aeronautics and Space Administration research centers and execution by two aerospace corporations was conducted efficiently with all the program goals achieved. The results validated and expanded on our knowledge of the causes and magnitude of short-term JT9D-7A engine performance deterioration.

5.2 FLIGHT LOADS

o The aerodynamic loads measured during take-off were the largest of any flight loads and were higher than previously predicted by Boeing for earlier analytical studies on the effects of flight loads on performance deterioration, Reference 3.

o The air stream inlet angle of attack with the fan inlet and the fan air flow rate determine the magnitude and direction of the aerodynamic load on the engine. These are, in turn, functions of airplane angle of attack, flap setting, air speed, and power setting.

o Inertial loads were less severe than previous studies had indicated and their effects were less then predicted.

5.3 CLEARANCE CLOSURES

o Maximum measured fan clearance closures occurred immediately following take-off rotation, concurrently with and in the direction of the maximum aerodynamic loads.

o Use of a 20-degree flap setting at take-off rather than 10-degree flaps reduced the aerodynamic load, the fan clearance closure, and thus the resultant fan seal rub. Hence, for a given take-off gross weight, 20-degree flaps resulted in less performance deterioration.

o There was no significant difference in aerodynamic loads and clearance closures between inboard and outboard engine fans for all flight conditions.

o Differential thermal expansion between case and rotor at high power was the prime cause of high-pressure turbine clearance closure. It combined with thrust- and aerodynamic load-induced case bending to maximize high-pressure turbine clearance closure during climb in the JT9D-7A test engine.

61

o   Extended, high power ground operation caused a maximum differential thermal expansion in the high-pressure turbine with resultant significant clearance closure. This condition should be avoided, especially prior to take-off, to prevent the effect of simultaneous maximum power- and aerodynamic load-induced closures.

o   In-flight engine decelerations followed by accelerations over a wide power range caused significant high-pressure turbine clearance closures, especially when the airplane was at a high angle of attack. This closure is due to the combined effects of the differential thermal expansion rate between disk and case and the peak aerodynamic load occurring during an acceleration at high airplane angle of attack.

o   Evaluation of the total high-pressure turbine clearance closure and the various contributing elements (that is, centrifugal, thermal, thrust, and aerodynamic loads) indicates that nonsymmetric thermal expansion effects are significant and worthy of further evaluation.

o   The dynamic load condition, the heavy gross weight, high sink rate landing had an insignificant effect on fan and high-pressure turbine running clearances.

5.4   PERFORMANCE EFFECTS

o   The fan and high-pressure turbine measured performance changes and estimated changes, based on past test hardware inspection, validated prior data for short-term rub-induced performance deterioration of those JT9D modules.

It should be noted that all phases of the NASA JT9D Jet Engine Diagnostics Program, including in-service data gathering, special testing, analysis, and performance deterioration modeling, utilized JT9D-7A engines. Thus the performance deterioration predictions, conclusions, and recommendations apply to engines with JT9D-7A technology. Knowledge gained from this program has and is currently being applied to achieve improved performance retention characteristics in later engine models.

SECTION 6.0

RECOMMENDATIONS

This section presents changes in engine operating procedures, design changes, and future investigative effort that should be considered to reduce the JT9D performance loss due to rubs.

6.1 FLIGHT PROCEDURES

It is suggested that modifications to flight procedures be considered in order to reduce high-load occurrences in both test (ground and flight acceptance testing and postrepair testing) and airline service.

o   During ground testing, extended high power operation should be curtailed, especially immediately preceding a take-off.

o   During airplane acceptance flight testing, recovery from the stall warning maneuver can result in lower load levels if engine thrust is not increased to maximum level upon recovery. This procedure may be feasible because the altitude loss under these conditions may not be a problem.

In airline service, use of the 20-degree flap setting, where allowable, and postponement of take-off rotation to a higher speed will tend to reduce the maximum inlet angle of attack, resulting in significant reductions in aerodynamic loads.

Deceleration-acceleration limitations presented Reference 5, Section 6 should be reviewed and followed.

6.2 FURTHER DESIGN AND DEVELOPMENT

The new recommendations following the Flight Loads Test are as follows:

o   Investigate methods of structurally integrating the engine and nacelle to reduce the asymmetric closure due to aerodynamic and thrust loads.

o   Investigate further the extent and cause of thermally-induced closures in the high-pressure turbine with the goal of minimizing nonsymmetric closures.

o   Continue development of gas-path clearance control systems and abradable rub strips to provide closer running clearances.

o   Investigate possible changes in production engine calibration testing of new and overhauled engines to reduce the time spent at high power and thus reduce high-pressure turbine clearance closure and resulting rubs.

Previous studies in the JT9D Engine Diagnostics Program have also resulted in design criteria and recommendations which are repeated here, where still applicable, for the sake of completeness:

o   Use derated power take-off when conditions permit to reduce hot section thermal distortion.

o   Develop improved erosion resistant coatings and materials for cold section airfoils and rub strips.

o   Develop designs to reduce ingestion of erosive materials into the compressor section of the engine.

o   Develop designs to reduce hot section temperature profile shifts and the resultant thermal distortion of gas-path parts.

o   Include clearance monitoring in the development testing of new engines.

o   Improve maintenance procedures.

These new and restated recommendations are discussed in greater detail in "Performance Deterioration due to Acceptance Testing and Flight Loads", Reference 2.

APPENDIX

ACRONYMS AND SYMBOLS

ACRONYMS (Oraganizations)

BCAC	Boeing Commercial Airplane Company
NASA	National Aeronautics and Space Administration
OPEC	Organization of Petroleum Exporting Countries
P&WA	Pratt & Whitney Aircraft

SYMBOLS

A, a	Acceleration
ACEE	Aircraft Energy Efficiency (Program)
ADAMS	Airborne Data Analysis and Monitoring System
CG	Airplane center of gravity
EAS	Equivalent air speed (knots, Mach number)
ECI	Engine Component Improvement (Program)
EGT	Exhaust gas temperature (°C)
EPR	Engine pressure ratio
EVC	Engine vane control
F	Force (pounds)
FN, Fn	Net thrust (pounds)
G, g	Gravity, gravitational constant
gyro	Gyroscopic, gyroscope
GW	Gross weight
HPC	High-pressure compressor
HPT	High-pressure turbine
Hz	Hertz
LPC	Low-pressure compressor
LPT	Low-pressure turbine
Max Q, q	Airplane maximum dynamic pressure
M	Moment (inch-pounds)
MN, Mn	Mach number
N	Rotor speed (rpm)
NAIL	Nacelle Aerodynamic and Inertial Loads (NASA Program)
NASTRAN	NASA STRuctural ANalysis (computer program)
P	Pressure (psia, lb/in^2)
q	Dynamic pressure
RPM, rpm	Revolutions per minute

SYMBOLS (Cont'd.)

SLS	Sea level static
SP	Special Performance (Boeing 747SP airplane)
T	Temperature (°F) (°C)
TOGW	Take-off gross weight (pounds)
TSFC	Thrust specific fuel consumption (lb/hr-lb)
W	Weight flow (lb/hr) (lb/min)
α	Inlet airflow angle of attack (degrees)
β	Vane angle (degrees)
Δ	Change
θ	Circumferential location (degrees)
ϕ, θ, ψ	Acceleration components

SUBSCRIPTS *

1	Undisturbed inlet (pressures and temperatures)
1	Low-pressure rotor (rotor speeds)
2	Fan inlet (pressures and temperatures)
2	High-pressure rotor (rotor speeds)
2.4	Fan blade discharge
2.5	Fan exit guide vane inlet
2.6	Fan exit guide vane discharge
3	Low-pressure compressor discharge
4	High-pressure compressor discharge
4.5	Combustor borescope location
5	High-pressure turbine inlet
6	High-pressure turibne discharge
7	Low-pressure turbine discharge
amb	Ambient
f	Fuel
i	Inner
S, s	Static
T, t	Stagnation (total)
x, y, z	Directional coordinates

---

* For simplicity, subscripts may be written "on the line" of type, especially in text.

REFERENCES

1. Martin, R. L.: Nacelle Aerodynamic and Inertial Loads (NAIL) Project, Test Report. NASA CR-165760, 1981.

2. Olsson, W. J: Performance Deterioration due to Acceptance Testing and Flight Loads. NASA CR-165572, 1982.

3. Jay, A. and Todd, E. S.: Effect of Steady Flight Loads on JT9D-7 Performance Deterioration. NASA CR-135407, 1978.

4. Sallee, G. P.: Performance Deterioration Based on Existing (Historical) Data. NASA CR-135448, 1978.

5. Olsson, W. J. and Sallee, G. P.: Performance Deterioration Based on In-Service Engine Data. NASA CR-159525, 1979.

6. Bouchard, R. J., Beyerly, W. R., and Sallee, G. P.: Short-Term Performance Deterioration in JT9D-7A(SP) Engine 695743. NASA CR-135431, 1978.

7. Jay, A. and Lewis, B. L.: Effect of Time-Dependent Flight Loads on JT9D-7 Performance Deterioration. NASA CR-159681, 1979.

8. Stromberg, W. J.: Performance Deterioration Based on Simulated Aerodynamic Loads Test. NASA CR-165297, 1981.

9. Sallee, G. P. and Martin, R. L.: Expanded Study of Feasibility of Measuring In-Flight 747/JT9D Loads, Performance, Clearance, and Thermal Data. NASA CR-159717, 1979.

10. An Approach to the Problem of Estimating Severe and Repeated Gust Loads for Missile Operations. NASA TN-4332, September 1958.